Article

Immunity

Stepwise epigenetic signal integration drives adaptive programming of cytotoxic lymphocytes

Graphical abstract

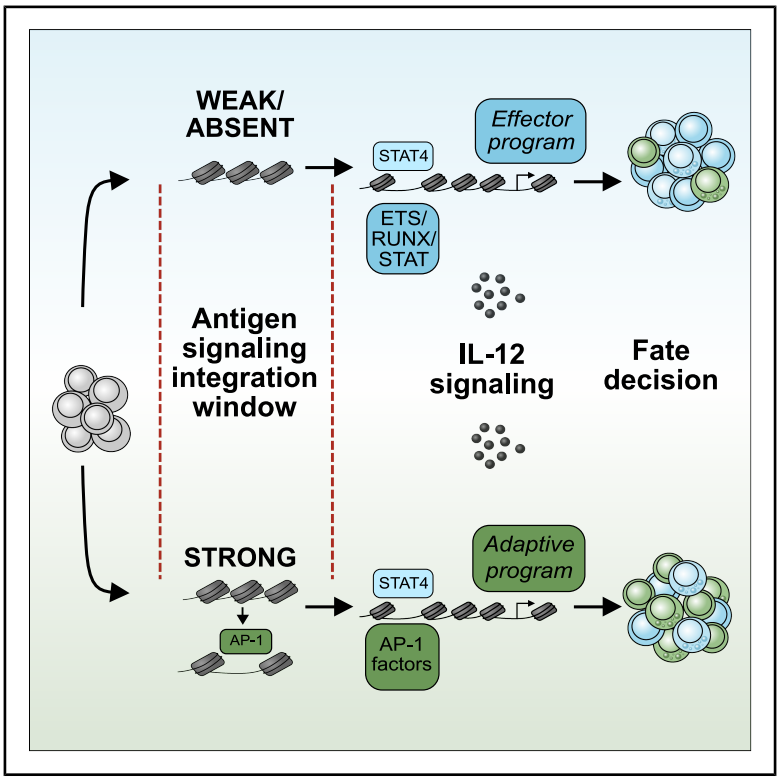

Authors

Simon Grassmann, Endi K. Santosa, Hyunu Kim, ..., Dirk H. Busch, Colleen M. Lau, Joseph C. Sun

Correspondence

grassmas@mskcc.org (S.G.), sunj@mskcc.org (J.C.S.)

In brief

Adaptive programming in lymphocytes during infection depends on when—not just whether—they sense antigen and proinflammatory cytokines such as IL-12. Grassmann et al. reveal that AP-1/STAT4 cooperation links signal timing to lymphocyte fate, tuning CD8$^+$ T cell responses and driving the decision between innate versus adaptive programs in NK cells.

Highlights

- Adaptive NK cell responses rely on sequential integration of antigen and cytokine signals
- Epigenetic redirection of STAT4 genomic binding promotes adaptive programming
- CD8$^+$ T cell fate depends on antigen-dependent integration of inflammatory signaling
- STAT/AP-1 cooperation underlies stepwise integration of antigen and cytokine signaling

Grassmann et al., 2026, Immunity *59*, 1–15
February 10, 2026
https://doi.org/10.1016/j.immuni.2026.01.004

CellPress

Immunity

CellPress

Article

Stepwise epigenetic signal integration drives adaptive programming of cytotoxic lymphocytes

Simon Grassmann,[1,13,*] Endi K. Santosa,[1,2,13] Hyunu Kim,[1,3] Isabelle B. Johnson,[1,2] Adriana M. Mujal,[1] Jean-Benoit LeLuduec,[4] Sherry X. Fan,[1,2] Mark Owyong,[1,2] Adrian Straub,[5] Liang Deng,[4,6,7] Katharine C. Hsu,[8,9,10] Dirk H. Busch,[5,11] Colleen M. Lau,[12] and Joseph C. Sun[1,2,14,*]

[1]Immunology Program, Memorial Sloan Kettering Cancer Center, New York, NY 10065, USA
[2]Department of Immunology and Microbial Pathogenesis, Weill Cornell Medical College, New York, NY 10065, USA
[3]Louis V. Gerstner Jr. Graduate School of Biomedical Sciences, Memorial Sloan Kettering Cancer Center, New York, NY 10065, USA
[4]Human Oncology and Pathogenesis Program, Memorial Sloan Kettering Cancer Center, New York, NY 10065, USA
[5]Institute for Medical Microbiology, Immunology and Hygiene, TUM School of Medicine and Health, Technical University of Munich (TUM), 81675 Munich, Germany
[6]Dermatology Service, Department of Medicine, Memorial Sloan Kettering Cancer Center, New York, NY 10065, USA
[7]Laboratory of Virology and Infectious Disease, The Rockefeller University, New York, NY 10065, USA
[8]Immuno-Oncology Program, Memorial Sloan Kettering Cancer Center, New York, NY 10065, USA
[9]Department of Medicine, Memorial Sloan Kettering Cancer Center, New York, NY 10065, USA
[10]Department of Medicine, Weill Cornell Medicine, New York, NY 10065, USA
[11]German Center for Infection Research (DZIF), Partner Site Munich, 81675 Munich, Germany
[12]Department of Microbiology and Immunology, College of Veterinary Medicine, Cornell University, Ithaca, NY 14853, USA
[13]These authors contributed equally
[14]Lead contact
*Correspondence: grassmas@mskcc.org (S.G.), sunj@mskcc.org (J.C.S.)
https://doi.org/10.1016/j.immuni.2026.01.004

SUMMARY

Lymphocyte differentiation during infection depends on the integration of antigen and cytokine signals, yet how the timing and sequence of these cues program cell fate remains unclear. We found that interleukin-12 (IL-12) plays a context-dependent role in immune memory formation. Without prior antigen-receptor signaling, IL-12 drove cytotoxic lymphocytes toward terminal effector differentiation. In contrast, antigen signaling redirected IL-12-STAT4 activity through cooperation with AP-1 transcription factors to promote memory formation. This stepwise signal integration enabled lymphocytes to acquire memory rather than effector fates. Whereas $CD8^+$ T cells were protected from premature IL-12 signaling by delayed receptor expression, natural killer (NK) cells, which constitutively express the IL-12 receptor, must engage their antigen receptor before cytokine signaling for efficient adaptive programming. Together, these findings define a framework in which sequential antigen and cytokine signaling coordinates effector versus memory differentiation, ensuring both robust primary responses and selective enrichment of high-avidity memory clones.

INTRODUCTION

Adaptive immune responses are crucial for protection against infections and cancer. During infection, immune cells must mount a robust effector response while also creating long-lived memory cells that protect against re-infection. Adaptive lymphocyte responses rely both on activating receptor and cytokine signaling.[1,2] How these signals are integrated to optimally tailor effector versus memory differentiation is incompletely understood. In T cells, antigen signaling and concomitant inflammatory cytokine signaling shape effector differentiation into memory precursors and short-lived effector cells.[3,4] Strong antigen-receptor signals promote both short-lived effector and memory differentiation to drive avidity maturation of memory T cell populations.[5] In contrast, inflammatory cytokines promote differentiation of short-lived effector cells[6]; however, their impact on memory precursor formation remains controversial. Inflammatory cytokine signals have been shown to either reduce,[7] promote,[8] or have no impact[9] on immunological memory in T cells, suggesting that other factors may influence how inflammatory cytokines affect T cell differentiation.

Recent findings have demonstrated that adaptive immune responses are not restricted to T and B cells of the adaptive immune system. Innate lymphocytes, such as natural killer (NK) cells, can mount robust adaptive responses during cytomegalovirus (CMV) infection in mice and humans.[10,11] Similar to T cells, adaptive NK cells rely on antigen-receptor signaling,[12,13] show antigen-dependent avidity maturation,[14,15] and require concomitant cytokine signals[16–18] for their clonal expansion and memory formation. Although NK cells express a variety of activating

Please cite this article in press as: Grassmann et al., Stepwise epigenetic signal integration drives adaptive programming of cytotoxic lymphocytes, Immunity (2026), https://doi.org/10.1016/j.immuni.2026.01.004

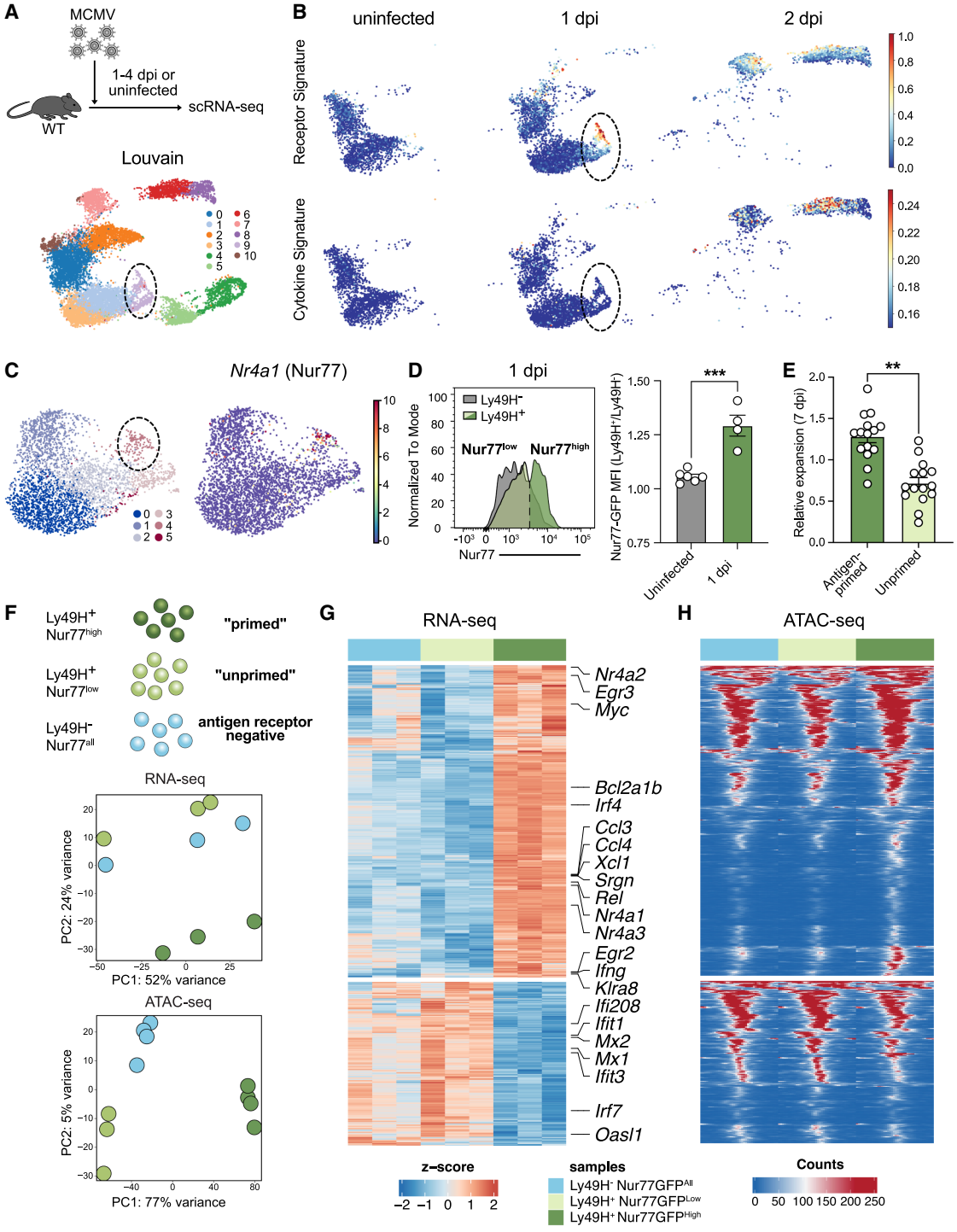

Figure 1. Adaptive NK cell responses rely on early antigen sensing *in vivo*

(A) Uniform manifold approximation and projection (UMAP) of single-cell transcriptomes of total NK cells (Ly49H$^+$ and Ly49H$^-$) and Louvain clustering of scRNA-seq and analysis of hashtag proportions in each identified cluster. Dotted line indicates cluster 9, showing earliest transcriptomic changes 1 dpi (one experiment).

(B) Cytokine and antigen receptor scores in scRNA-seq, separated according to dpi.

(C) Left: isolated Louvain clustering of single-cell transcriptomes from 1 dpi. Dotted line indicates cluster 4, corresponding to cluster 9 in the full dataset. Right: expression of *Nr4a1* in UMAP.

(D) Nur77-GFP signal in uninfected mice ($n = 6$) and 1 dpi ($n = 4$). MFI ratios of Nur77-GFP in Ly49H$^+$ and Ly49H$^-$ NK cells 1 dpi. Quantification of Nur77GFP MFI in antigen-receptor-positive and -negative NK cells (ratio Ly49H$^+$/Ly49H$^-$).

(legend continued on next page)

Please cite this article in press as: Grassmann et al., Stepwise epigenetic signal integration drives adaptive programming of cytotoxic lymphocytes, Immunity (2026), https://doi.org/10.1016/j.immuni.2026.01.004

receptors,[19,20] CMV infection is the main driver of such adaptive responses in NK cells. This suggests that CMV infection provides either a unique combination or sequence of signals leading to adaptive responses by otherwise innate lymphocytes. Originally, it was proposed that NK cells during mouse cytomegalovirus (MCMV) infection first participate in a cytokine-driven innate response before mounting their adaptive responses.[12] However, the exact sequence of antigen and cytokine signals has not been tested *in vivo*. We hypothesize that understanding the molecular events underlying adaptive NK cell responses during CMV infection can elucidate the core principles of lymphocyte adaptive responses. In our study, we find that adaptive NK cell responses rely on sequential and epigenetic integration of antigen and signal transducer and activator of transcription 4 (STAT4) signaling. By the same mechanism, STAT4 shapes the fate decisions of high- and low-avidity CD8$^+$ T cells.

RESULTS

Adaptive NK cells sense antigen prior to inflammatory cytokine signaling

Because proinflammatory cytokine signals are crucial for lymphocyte responses in addition to antigen-receptor signals,[16–18] we hypothesized that either one of two mechanisms mediates signal integration (Figure S1A): (1) priming of lymphocytes involves concomitant antigen-receptor and cytokine signaling (simultaneous integration) or (2) antigen-receptor and cytokine signaling occur sequentially (sequential integration). To determine how antigen and cytokine signals are integrated during adaptive NK cell responses, we analyzed the precise sequence of signaling events in NK cells during MCMV infection using single-cell RNA sequencing (scRNA-seq) (Figures 1A and S1B). The time course revealed a cluster containing the earliest virus-specific transcriptomic changes 1 day post-infection (1 dpi) compared with uninfected mice (Figures 1B and S1B). Using a cytokine signaling score[21] versus an antigen-receptor signaling score (Figures S1C and S1D), we observed that the earliest transcriptomic changes found 1 dpi were best characterized by antigen-receptor signaling. Robust expression of cytokine-dependent genes did not appear until 2 dpi. Together, these data suggest that antigen-receptor signals are integrated before cytokine signals in a subset of NK cells during MCMV infection. The earliest detectable transcriptomic changes included the gene encoding the antigen receptor Ly49H and genes induced by antigen-receptor signaling, such as Nr4a and Egr-family members (Figures 1C and S1F).

Because *Nr4a1*, a well-known target of antigen-receptor signaling[22] (Figure 1C), was upregulated 1 dpi, we used the *Nr4a1* (Nur77) GFP reporter mouse[23] to study the fate of early antigen-primed NK cells. Under steady state, Ly49H$^-$ and Ly49H$^+$ NK cells showed similar mean fluorescence intensity (MFI) of Nur77 (Figure S1G). In accordance with the scRNA-seq kinetics, Ly49H$^+$ NK cells induced Nur77-GFP as early as 1 dpi, with GFP expression enriched in antigen-receptor positive (Ly49H$^+$) NK cells compared with antigen-receptor negative (Ly49H$^-$) NK cells (Figure 1D). Nur77-reporter expression and scRNA-seq revealed that not all Ly49H$^+$ NK cells received this early antigen-receptor signal, suggesting that there are antigen-receptor-primed and -unprimed NK cells within the Ly49H$^+$ population 1 dpi. To test whether these two groups differed in their capacity for clonal expansion, we co-transferred equal numbers of Nur77^{high} and Nur77^{low} NK cells at 1 dpi into infection-matched mice and measured their relative numbers 7 days later. In this direct comparison, Nur77^{high} NK cells showed greater expansion than Nur77^{low} NK cells (Figure 1E). Thus, the population of early antigen-primed NK cells represented the main source of the adaptive NK cell pool.

Next, we performed RNA sequencing (RNA-seq) and assay for transposase-accessible chromatin using sequencing (ATAC-seq) on three subsets of NK cells 1 dpi: Ly49H$^-$ (antigen-receptor-negative), Ly49H$^+$ Nur77^{high} (antigen-primed), and Ly49H$^+$ Nur77^{low} (unprimed) NK cells (Figure 1F). Ly49H$^+$ Nur77^{high} NK cells showed a transcriptional and epigenetic profile distinct from both Ly49H$^+$ Nur77^{low} and Ly49H$^-$ NK cells (Figures 1G and 1H), which were similar. Furthermore, this Nur77^{high} profile strongly mapped to the observed transcriptomic changes by scRNA-seq 1 dpi, and was enriched in a distinct cluster 2 dpi, likely representing antigen-primed NK cells at this time point (Figures S2A and S2B). Ly49H$^+$ Nur77^{high} NK cells showed enrichment of antigen-dependent genes and pathways but reduced expression of genes from cytokine pathways (Figure S2C). Moreover, comparison of transcriptomic and epigenetic changes in Ly49H$^+$ Nur77^{high} NK cells with *in vitro*-stimulated NK cells suggested a high degree of correlation only with antigen-receptor signaling (Figures S2D–S2G). Together, our data favor the sequential signal integration model, in which antigen receptor engagement occurs before cytokine signaling to drive adaptive NK cell responses.

Antigen-receptor signals redirect STAT4 genomic binding toward AP-1 sites

To assess whether antigen-receptor signaling altered genomic sites bound by cytokine-dependent STAT transcription factors (TFs), we compared differentially accessible regions in early antigen-primed NK cells with STAT1, STAT4, and STAT5 chromatin immunoprecipitation sequencing (ChIP-seq) datasets from cytokine-stimulated NK cells.[21] Nur77^{high} NK cells showed an

(E) Co-transfer of congenically marked Ly49H$^+$ Nur77-GFP^{high} and Ly49H$^+$ Nur77-GFP^{low} NK cells into infection-matched Ly49H$^{-/-}$ mice and measurement of expansion (n = 15). Relative expansion is calculated by dividing percentage at the time of the analysis by percentage at the time of the injection for comparison between multiple experiments (e.g., 75% 7 dpi and 50% at time of injection: 75%/50% = 1.5).
(F) Sort of Ly49H$^+$ Nur77^{high}, Ly49H$^+$ Nur77^{low}, and Ly49D$^+$ Ly49H$^-$ NK cells 1 dpi. Principal-component analysis (PCA) plots of RNA-seq (n = 3) and ATAC-seq (n = 3–4) from Ly49H$^+$ Nur77^{high}, Ly49H$^+$ Nur77^{low}, and Ly49D$^+$ Ly49H$^-$ NK cells 1 dpi. (One experiment).
(G) Heatmap of RNA-seq of Ly49H$^+$ Nur77^{high}, Ly49H$^+$ Nur77^{low}, and Ly49D$^+$ Ly49H$^-$ NK cells.
(H) Heatmap of ATAC-seq of Ly49H$^+$ Nur77^{high}, Ly49H$^+$ Nur77^{low}, and Ly49D$^+$ Ly49H$^-$ NK cells.
Data in (D) and (E) are pooled from two individual experiments. Error bars represent SEM. Significances are calculated as unpaired or paired t test. ****$p < 0.0001$, ***$p < 0.001$, **$p < 0.01$, *$p < 0.05$.
See also Figures S1 and S2.

Please cite this article in press as: Grassmann et al., Stepwise epigenetic signal integration drives adaptive programming of cytotoxic lymphocytes, Immunity (2026), https://doi.org/10.1016/j.immuni.2026.01.004

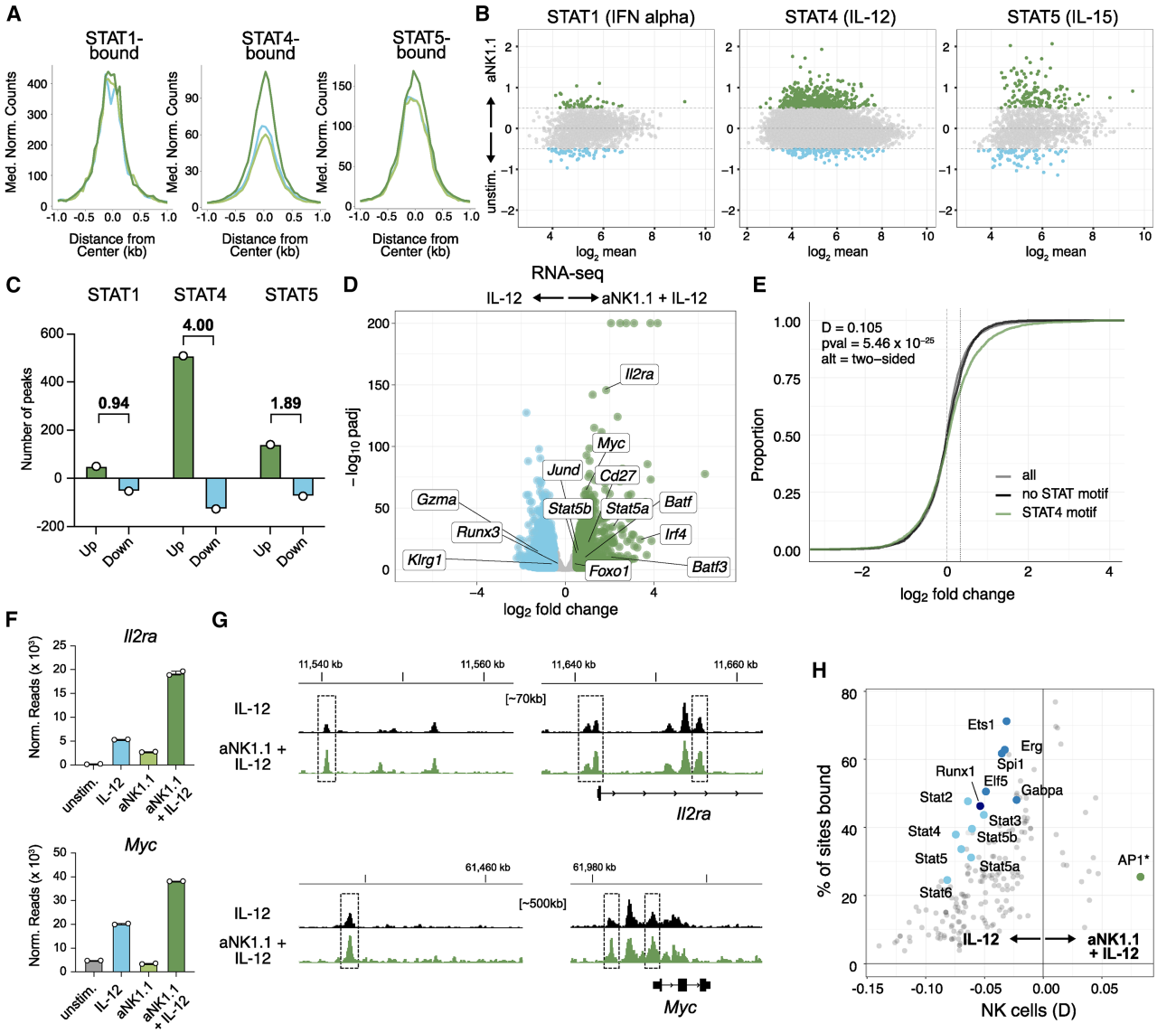

Figure 2. Antigen priming modulates subsequent cytokine signaling by altering STAT4 genomic binding

(A) Comparison of accessibility of STAT1, STAT4, and STAT5 binding peaks as assessed with ChIP-seq. Dark green: Ly49H^{+} Nur77^{high}. Light green: Ly49H^{+} Nur77^{low}. Light blue: Ly49H^{-}.

(B) NK cells were pre-stimulated with antigen or left untreated. After 3 h, NK cells were stimulated with IFN-α, IL-12, or IL-15, and STAT1, STAT4, or STAT5 CUT&RUN, respectively, were performed and analyzed with median-of-ratios normalization. MA plots show mean read count (*x* axis) and $\log_2$ fold change between the two conditions (*y* axis). Peaks with a $\log_2$ fold change > 0.5 were highlighted. (n = 2 for STAT1 and STAT5, n = 3 for STAT4, one experiment).

(C) Quantification of the number of peaks with $\log_2$ fold change > 0.5 in (B). Numbers indicate ratios of the peak number that showed positive versus negative $\log_2$ fold change.

(D) Volcano plot of differential gene expression in IL-12-stimulated and aNK1.1+IL-12-stimulated NK cells (n = 2, one experiment).

(E) Empirical cumulative distribution function (ECDF) plot of genes that show differential STAT4 binding. Statistics are derived from Kolmogorov-Smirnov (KS) test. Genes that showed antigen-dependent STAT4 binding were subset into regions that contained a STAT motif or not to discern direct from indirect STAT4 genomic binding. Genes that showed antigen-dependent STAT4 binding and contained a STAT motif showed increased expression in RNA-seq (IL-12 versus aNK1.1 + IL-12).

(F) Example reads for *Il2ra* and *Myc*.

(G) Normalized STAT4 CUT&RUN tracks averaged across all replicates for *IL2ra* and *Myc* loci in IL-12-stimulated (black) and aNK1.1+IL-12-stimulated (green) NK cells.

(H) Motif enrichment plot. Peaks with antigen-dependent increase and decrease in STAT4 binding in IL-12 and aNK1.1 + IL-12-stimulated NK cells were compared with the total STAT4 atlas to examine motif enrichment using one-sided KS test. The KS test statistic D is shown on the *x* axis and the proportion of regions associated with the motif is shown on the *y* axis. The odds ratio (frequency of the motif in the increase or decrease group divided by its frequency in the

(legend continued on next page)

Please cite this article in press as: Grassmann et al., Stepwise epigenetic signal integration drives adaptive programming of cytotoxic lymphocytes, Immunity (2026), https://doi.org/10.1016/j.immuni.2026.01.004

enrichment of regions that were bound by STAT4 and, to a lesser degree, STAT5 (Figure 2A). To directly test whether antigen stimulation redirects STAT1, STAT4, and STAT5, we sequentially stimulated NK cells with antigen followed by specific STAT-activating cytokines (i.e., interferon [IFN]-α for STAT1, interleukin [IL]-12 for STAT4, and IL-15 for STAT5) and performed CUT&RUN analysis (Figure 2B). For antigen stimulation, we selected aNK1.1 because signaling through NK1.1 and Ly49H elicits similar transcriptomic and epigenetic changes in NK cells (Figure S2H), but anti-Ly49H would only trigger half of the NK cell population. Of the three STATs, STAT4 showed the most pronounced increase in genomic binding (Figure 2C), confirming our *in silico* prediction.

The observed redistribution of STAT4 binding following prior antigen stimulation suggested that antigen signaling altered subsequent IL-12 signaling. To match genomic STAT4 binding to gene expression, we stimulated antigen-receptor pre-stimulated or control NK cells with IL-12 and performed RNA-seq (Figures 2D, S3A, and S3B). Genes bound by STAT4 showed altered gene expression dependent on direct STAT4 binding, as genes with STAT4 binding that did not harbor a STAT motif (likely via indirect binding) did not show such regulation (Figure 2E). Among the top genes differentially expressed between IL-12-stimulation alone versus sequentially stimulated NK cells, we found several genes crucial for adaptive NK cell responses, including *Myc*,[24] *Irf4*,[25] *Stat5a*, *Stat5b*, and the high-affinity IL-2 receptor *IL2ra*[16] (Figure 2D). For many of these genes, sequential stimulation increased expression beyond what would be expected if the signals were additive (Figure 2F), and antigen-receptor signaling redirected STAT4 genomic binding (Figures 2G and S3C). We speculated that differentially bound loci harbor distinct TF-binding motifs. Indeed, regions with an antigen-dependent decrease in STAT4 binding were relatively enriched for erythroblast transformation specific (ETS), Runt-related transcription factor (RUNX), and STAT motifs, whereas regions with an antigen-dependent increase in STAT4 genomic binding were particularly enriched for activator protein 1 (AP-1) motifs (Figures 2H and S3D). Thus, our data show that antigen-receptor signaling redirects STAT4 genomic binding away from ETS, RUNX, and STAT motifs and toward AP-1 binding sites.

AP-1 acts as a pioneer factor to enable AP-1/STAT4 cooperation

To further understand how regions containing AP-1 motifs increase STAT4 genomic binding, we performed STAT4 CUT&RUN in the presence of a pan-AP-1 inhibitor (AP1i) (Figures 3A–3C, S4A, and S4B). Pre-incubation of NK cells with AP1i specifically reduced antigen-dependent STAT4 genomic binding in peaks containing AP-1 motifs (e.g., peaks 2,621 and 3,254) but not in peaks without AP-1 motifs (Figures 3A and 3B, e.g., peaks 2,616–2,619 and 3,252–3,253). AP-1 factors have been proposed to act as pioneer factors regulating chromatin accessibility.[26] To test whether antigen signaling alters chromatin accessibility via AP-1, we performed ATAC-seq of NK cells stimulated with antigen receptor in the presence or absence of AP1i (Figures 3D, 3E, and S4C). In addition, we conducted CUT&RUN for c-Jun to directly visualize AP-1 binding (Figures 3D, 3E, and S4D), as c-Jun was expressed at higher levels than other AP-1 family members and was induced by antigen stimulation in NK cells (Figure 4E). Regions where AP-1 inhibition reduced STAT4 genomic binding showed AP1-dependent changes in chromatin accessibility and c-Jun binding (Figures 3D, 3E, and S4F). Globally, regions that bound c-Jun after antigen stimulation gained accessibility (Figures 3F and S4G) and showed increased STAT4 genomic binding after subsequent IL-12 stimulation (Figures 3G and S4H). In summary, our findings suggest that antigen priming leads to AP-1-dependent chromatin changes that facilitate genomic relocation of STAT4 (Figure 3H).

Stepwise signal integration is required for an adaptive fate decision in NK cells

Our data indicated that antigen signaling redirects STAT4 genomic binding, suggesting that IL-12 signaling may differentially impact NK cells, with or without the antigen receptor Ly49H. Indeed, whereas IL-12 signaling was crucial for efficient adaptive NK cell responses in the Ly49H$^+$ subset (Figures 4A and S4I),[17] IL-12 signaling impaired expansion of Ly49H$^-$ (i.e., antigen-receptor-negative) NK cells (Figures 4B and S4J). This inverse impact of IL-12 on antigen-receptor-expressing or -negative cells was visible as early as 4 dpi, marking the beginning of adaptive NK cell responses (Figure S4K).[27] We hypothesized that, in the absence of prior antigen signaling, IL-12 may lead to terminal instead of adaptive differentiation of NK cells, explaining the context-dependent impact on expansion. Indeed, without prior antigen-receptor signaling, IL-12 impaired NK cell proliferation in *in vitro* assays (Figures 4C–4F), and pre-incubating NK cells with IL-12 impaired their adaptive potential *in vivo* (Figure 4G). Because IL-12 exposure in the absence of antigen signals completely arrested proliferation in many NK cells, we attempted to find evidence for this proliferation arrest in our Nur77 system. Indeed, CellTrace Violet (CTV) labeling of co-transferred Ly49H$^+$ Nur77^{high} (primed) and Ly49H$^+$ Nur77^{low} (unprimed) NK cells revealed an accumulation of undivided NK cells within the transferred Nur77^{low} NK cell population (Figure 4H).

Together, our analysis of adaptive NK cell responses suggests that differential integration of inflammatory cytokine signals promotes distinct fate decisions in NK cells: without prior antigen signaling, STAT4 induces terminal differentiation of NK cells incapable of proliferation by binding to genomic regions shared with RUNX and ETS motifs (Figure 4I). Sufficient antigen-receptor signaling redirects subsequent STAT4 genomic binding toward AP-1 binding sites, instead promoting adaptive programming of NK cells (Figure 4I).

Integration of inflammatory cytokine signals in CD8$^+$ T cells depends on antigen strength

Previously, we have found shared epigenetic features in the adaptive programming of innate and adaptive lymphocytes.[28] Naive

entire atlas) was used to assign the motif to either the left (regions with antigen-dependent decrease, negative value) or the right (regions with antigen-dependent increase, positive value) on the *x* axis. All motifs (224) from JASPAR CORE(v2024) *Mus musculus* database were analyzed. Each color represents motif families as mentioned (STAT, RUNX, and ETS motifs). *AP-1 motif labeled here overlaps three motifs, Atf3, Jun, and Fos::Jun.
See also Figure S3 and Table S1.

Please cite this article in press as: Grassmann et al., Stepwise epigenetic signal integration drives adaptive programming of cytotoxic lymphocytes, Immunity (2026), https://doi.org/10.1016/j.immuni.2026.01.004

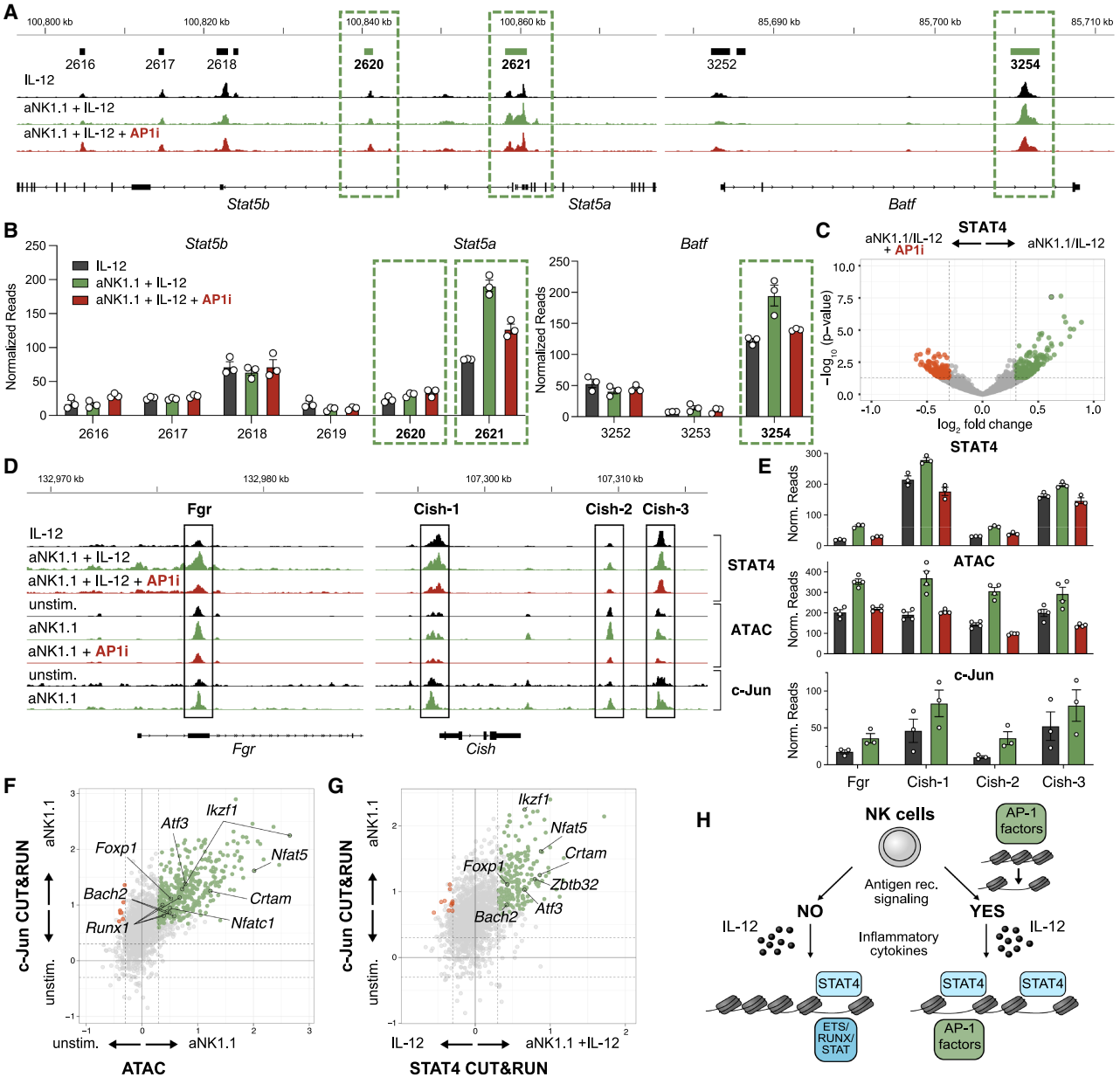

Figure 3. AP-1 acts as pioneer factor to redirect STAT4 genomic binding in adaptive NK cells

(A) NK cells were stimulated with IL-12, aNK1.1 + IL-12, or AP1i + aNK1.1 + IL-12 (stimulation sequence: ±AP1i → ±aNK1.1 → ±IL-12, also see Figure S5A for experimental setup). Normalized STAT4 CUT&RUN tracks averaged across all replicates are shown. Peaks are denoted as a bar above the tracks with a peak ID, and peaks with a green bar and outlined with a green dotted line contain AP-1 motifs (n = 3 pools of three mice each, one experiment).

(B) Quantification of normalized read counts from peaks shown in (A). Boxes with dotted line indicate peaks containing AP-1 motifs from (A).

(C) Volcano plot of STAT4 genomic binding after aNK1.1 + IL-12 versus AP1i + aNK1.1 + IL-12 stimulation. Highlighted are regions with $p < 0.05$ and $\log_2$ fold change > 0.3.

(D) Example peaks for STAT4 CUT&RUN, ATAC-seq, and c-Jun CUT&RUN (normalized with flanking method) in the indicated conditions.

(E) Quantification of peaks shown in (D).

(F) Scatterplot between the overlapping peaks of ATAC-seq and c-Jun CUT&RUN for NK cells stimulated with aNK1.1 versus unstimulated control.

(G) Scatterplot between the overlapping peaks of STAT4 CUT&RUN and c-Jun CUT&RUN for stimulated NK cells versus control in the respective conditions.

(H) Schematic of STAT4 genomic binding in antigen-primed and antigen-unprimed NK cells.

See also Figure S4.

Please cite this article in press as: Grassmann et al., Stepwise epigenetic signal integration drives adaptive programming of cytotoxic lymphocytes, Immunity (2026), https://doi.org/10.1016/j.immuni.2026.01.004

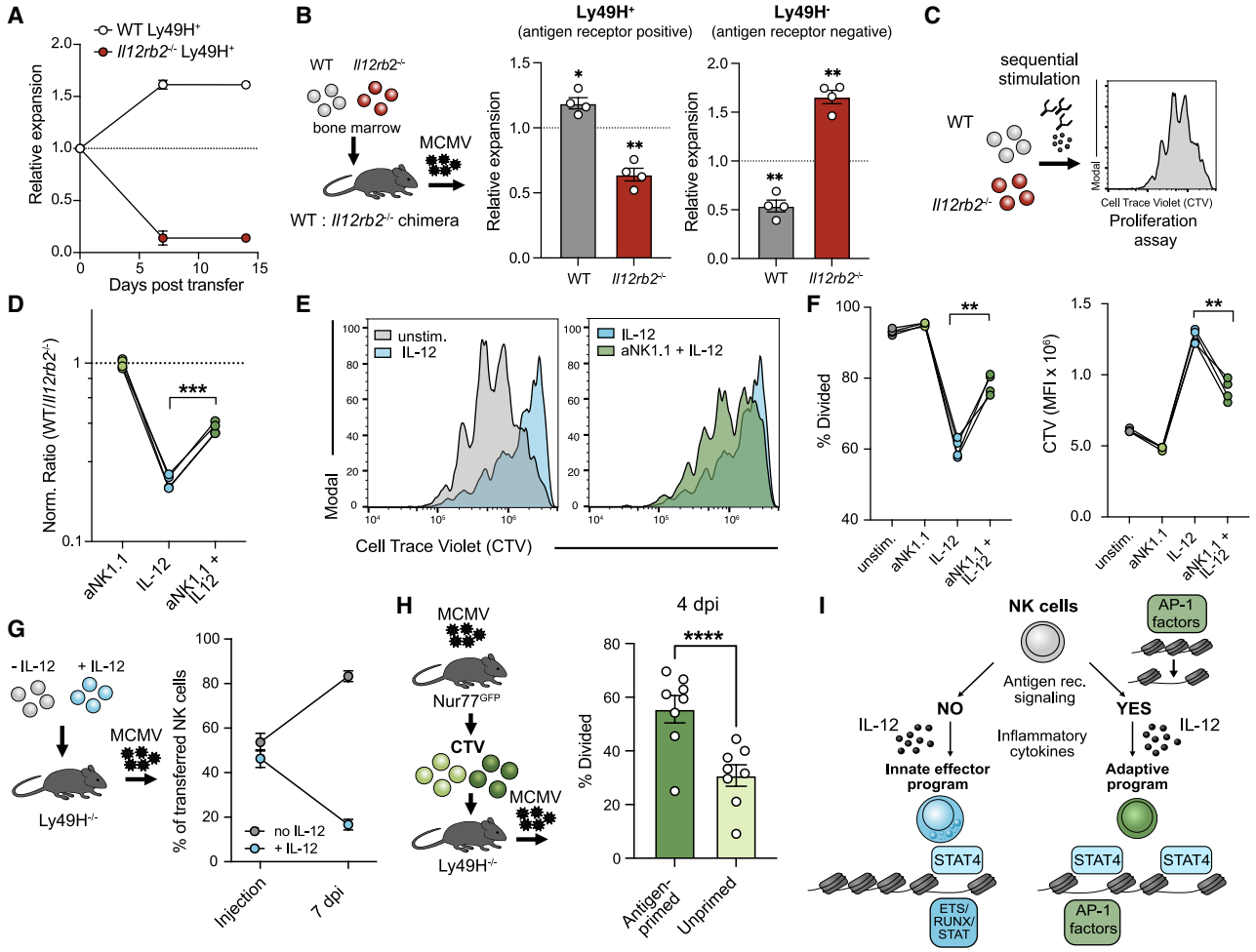

Figure 4. Early antigen signaling promotes innate versus adaptive fate decision in NK cells

(A) Adoptive co-transfer of WT and *Il12rb2*$^{-/-}$ NK cells into Ly49H-deficient hosts and measurement of expansion following MCMV infection (n = 8).

(B) Expansion of NK cells in competitive WT:*Il12rb2*$^{-/-}$ chimera 7 dpi separated into Ly49H^{+} (antigen-receptor expressing) and Ly49H^{-} (antigen-receptor negative) NK cells (n = 4).

(C) Schematic of CTV dilution proliferation assay.

(D) Relative abundance of WT and *Il12rb2*$^{-/-}$ NK cells in IL-12, anti-NK1.1, or sequentially stimulated NK cells after 3 days of stimulation with IL-15 (n = 4).

(E) Representative histograms showing CTV dilution in an IL-15-dependent proliferation assay.

(F) Quantification of divided cells and CTV MFI.

(G) Co-transfer of untreated or IL-12 pre-incubated NK cells into Ly49H$^{-/-}$ mice infected with MCMV and measurement of expansion (n = 7).

(H) Nur77^{high} (antigen-primed) and Nur77^{low} (unprimed) NK cells 1 dpi from Nur77-GFP mice were isolated, stained with CTV, and co-transferred into infection-matched recipients. Measurement of division 4 dpi (n = 8).

(I) Schematic of fate decision between the innate effector program and the adaptive program via differential integration of inflammatory signaling in antigen-receptor-positive and -negative NK cells.

Data in (A), (B), (G), and (H) are pooled from two individual experiments. Data in (D) and (F) are representative of two individual experiments. Error bars represent SEM. Significances are calculated as paired t test (competitive chimera, co-transfers, or the same biological replicates). ****p < 0.0001, ***p < 0.001, **p < 0.01, *p < 0.05.

See also Figure S4.

CD8^{+} T cells do not express the IL-12 receptor until activation,[29] making it impossible to study the impact of IL-12 signaling in T cells that have not seen antigen. Thus, we instead hypothesized that, in CD8^{+} T cells, the strength of antigen signaling (rather than the presence or absence of the antigen receptor) may influence subsequent cytokine signaling. To test this idea, we generated retrogenic mice from wild-type (WT) or *Il12rb2*$^{-/-}$ stem cells transduced with a high- or low-affinity T cell receptor (TCR) from a previously generated library of SIINFEKL peptide-specific TCRs[30] (Figure S5A). When retrogenic T cells were transferred into mice infected with recombinant *Listeria monocytogenes* expressing SIINFEKL (*L.m.*-SIINFEKL), IL-12 promoted clonal expansion in high-avidity (B11) but not low-avidity (E8) CD8^{+} T cells (Figure 5A). When comparing memory responses after challenge with the heterologous pathogen MVAΔE5R-OVA,[31] high-avidity T cells similarly showed a greater recall potential,

Please cite this article in press as: Grassmann et al., Stepwise epigenetic signal integration drives adaptive programming of cytotoxic lymphocytes, Immunity (2026), https://doi.org/10.1016/j.immuni.2026.01.004

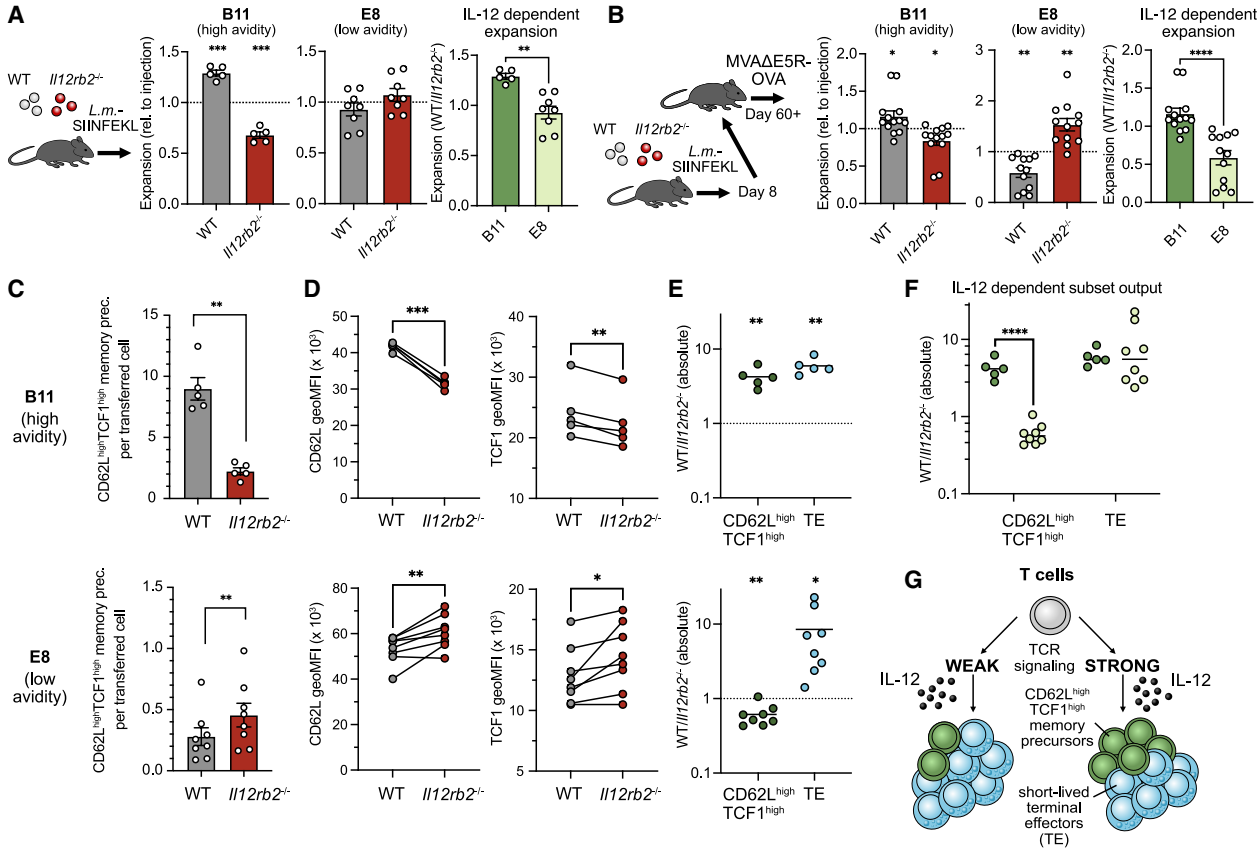

Figure 5. Avidity-dependent integration of inflammatory cytokine signaling drives CD8⁺ T cell differentiation

(A) Left: acute expansion (day 8) of high-avidity (B11) and low-avidity (E8) WT and *Il12rb2*$^{-/-}$ CD8⁺ T cells in mice infected with *L.m.*-SIINFEKL. Right: comparison of WT/*IL12rb2*$^{-/-}$ ratios of absolute per-cell output for high- and low-avidity T cells during the acute response (n = 5 for B11, n = 8 for E8).

(B) Left: recall expansion of high-avidity (B11) and low-avidity (E8) WT and *Il12rb2*$^{-/-}$ CD8⁺ T cells during recall response against MVAΔE5R-OVA. Retransfer of whole splenocytes into secondary recipients 8 dpi and recall infection after >60 days post transfer. Right: comparison of WT/*Il12rb2*$^{-/-}$ ratios of absolute per-cell output for high- and low-avidity T cells (n = 13 for B11, n = 12 for E8).

(C) Comparison of WT and *Il12rb2*$^{-/-}$ CD62L^{high}TCF1^{high} memory precursor output per transferred cell for high-avidity (top, B11) and low-avidity (bottom, E8) T cells during the acute response against *L.m.*-SIINFEKL.

(D) CD62L and TCF1 MFIs of CD62L⁺ T cells derived from high-avidity (top, B11) and low-avidity (bottom, E8) WT and *Il12rb2*$^{-/-}$ CD8⁺ T cells.

(E) WT/*Il12rb2*$^{-/-}$ ratio of absolute cell output for CD62L^{high}TCF1^{high} memory precursor and terminal effector (TE) cells for high-avidity (top, B11) and low-avidity (bottom, E8) T cells.

(F) Direct comparison of IL-12-dependent CD62L^{high}TCF1^{high} memory precursor and TE output for high-avidity (dark green, B11) and low-avidity (light green, E8) T cells.

(G) Schematic: antigen signal strength directs inflammation-dependent fate decision between memory and effector fates in high- and low-avidity CD8⁺ T cells.

Data in (A) and (C)–(F) are representative of 2–3 independent, similar experiments. Data in (B) are pooled from two individual experiments. Error bars represent SEM. Significances are calculated using paired or unpaired t test. ****$p < 0.0001$, ***$p < 0.001$, **$p < 0.01$, *$p < 0.05$.

See also Figure S5.

dependent on IL-12. In contrast, low-avidity T cells with intact IL-12 signaling had impaired memory responses (Figure 5B).

We hypothesized that the observed differences in memory potential were due to differential generation of memory precursor populations (Figure S5B). Using different marker combinations, we confirmed previous studies that showed defective differentiation of terminal effector cells by *Il12rb2*$^{-/-}$ T cells[6,7] (Figures S5C and S5D). Comparing memory precursor populations, only high-avidity T cells showed an increase in differentiation into CD62L^{high} TCF1^{high} memory precursor cells[32,33] (Figures S5D and S5E). On average, WT high-avidity T cells generated far more CD62L^{high} TCF1^{high} memory precursor cells than *Il12rb2*$^{-/-}$ counterparts (9.0 versus 2.0, Figure 5C, top). However, among low-avidity T cells, WT cells generated fewer CD62L^{high} TCF1^{high} memory precursors than *Il12rb2*$^{-/-}$ controls (0.28 versus 0.45, Figure 4C, bottom). In general, CD62L⁺ WT cells showed higher expression of CD62L and TCF1 than *Il12rb2*$^{-/-}$ counterparts (Figure 5D, top), whereas the opposite was observed in low-avidity T cells (Figure 5D, bottom).

Quantifying the IL-12-dependent output of subsets (WT:*Il12rb2*$^{-/-}$ ratio), terminal effector cell output was similarly dependent on IL-12 signaling in both high- and low-avidity T cells (Figures 5E and 5F). CD62L^{high} TCF1^{high} memory

Please cite this article in press as: Grassmann et al., Stepwise epigenetic signal integration drives adaptive programming of cytotoxic lymphocytes, Immunity (2026), https://doi.org/10.1016/j.immuni.2026.01.004

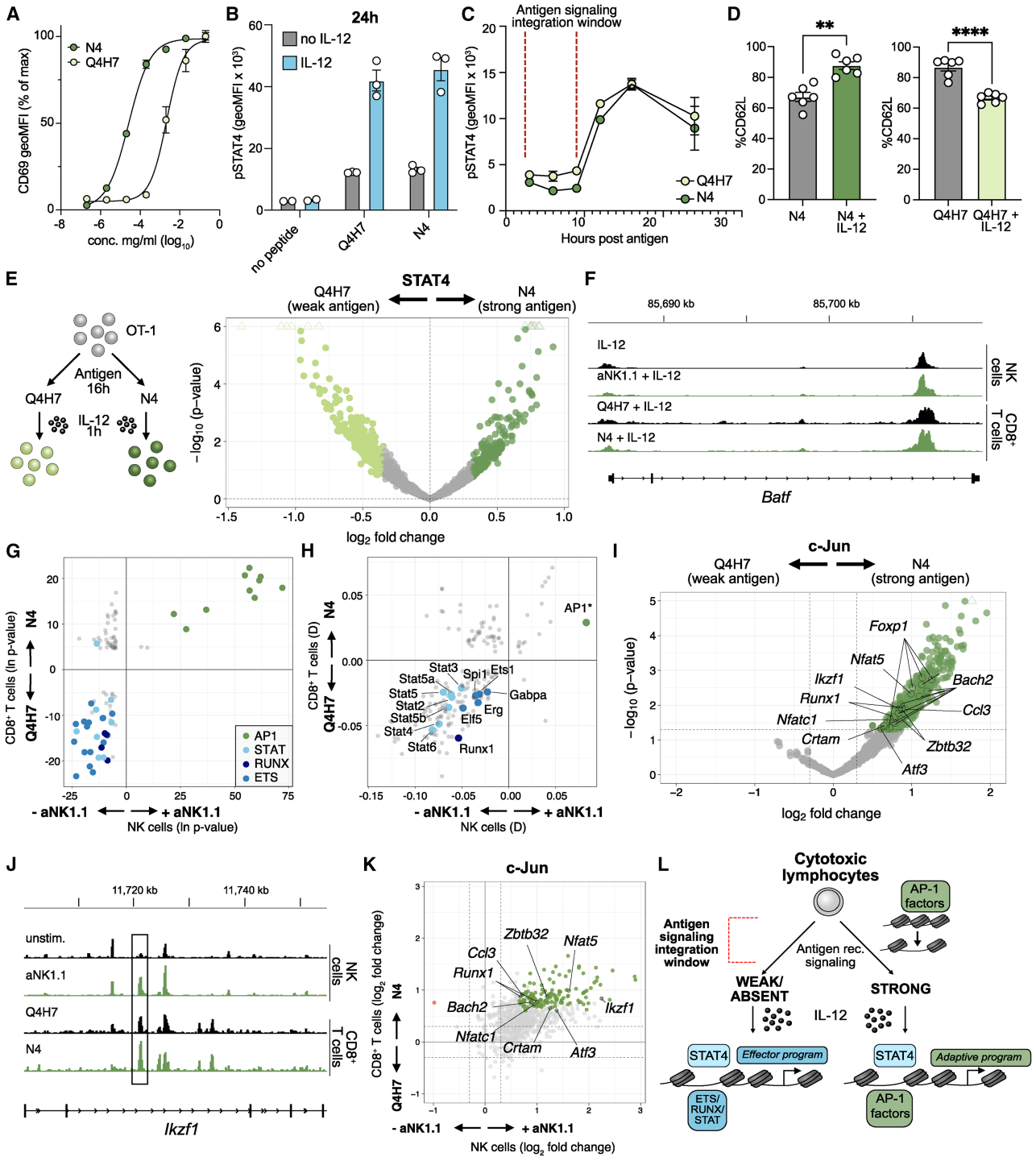

Figure 6. Sequential integration via STAT/AP-1 cooperation shapes effector versus memory differentiation in cytotoxic lymphocytes

(A) Peptide titration of SIINFEKL (N4, high avidity) and SIIQFEHL (Q4H7, low avidity)[34] stimulated OT-1 T cells (n = 2).

(B) pSTAT4 staining of IL-12 stimulated T cells after 24 h of peptide stimulation (10 ng/ml) (n = 3).

(C) Time titration of pSTAT4 MFI after 1 h of IL-12 stimulation of peptide stimulated OT-1 T cells (n = 3).

(D) Flow cytometry analysis of CD62L expression levels (measured as MFI) after 3 days of high- and low-avidity peptide ±/− IL-12 (n = 6).

(E) Volcano plot of STAT4 CUT&RUN differential binding analysis using median-of-ratios normalization. Light green indicates the top 20% of peaks by absolute $\log_2$ fold change that increase in binding upon weak antigen compared with strong antigen stimulation. Dark green indicates the top 20% of peaks by absolute

(legend continued on next page)

Please cite this article in press as: Grassmann et al., Stepwise epigenetic signal integration drives adaptive programming of cytotoxic lymphocytes, Immunity (2026), https://doi.org/10.1016/j.immuni.2026.01.004

precursor cells, however, were generated in an IL-12-dependent manner in high- but not low-avidity T cells. Thus, in $CD8^+$ T cells, antigen-receptor signal strength resulted in differential integration of subsequent inflammatory signals. This mechanism led to a preferential accumulation of $CD62L^{high}$ $TCF1^{high}$ memory precursors and increased memory potential in high-avidity T cells, whereas the output of short-lived effector cells was not impacted by avidity (Figure 5G).

Stepwise signal integration is a conserved feature in innate and adaptive lymphocytes

Our data revealed a context- and antigen-dependent role for IL-12 in both NK cells and $CD8^+$ T cells. To test whether antigen-receptor signaling in T cells redirects STAT4 genomic binding as observed for NK cells, we set up an *in vitro* model of sequential stimulation. To mimic high-avidity and low-avidity TCR signaling, we used altered peptide ligands for SIINFEKL-specific OT-I T cells,[34] and titration of peptides revealed an avidity-dependent upregulation of the activation marker CD69 (Figure 6A). Because $CD8^+$ T cells do not express the IL-12 receptor until activation via the TCR,[29] we assessed the earliest time point at which $CD8^+$ T cells can detect IL-12 signaling. A kinetic experiment revealed that both high- and low-avidity T cells first begin to show IL-12-dependent pSTAT4 at 12–16 h following peptide stimulation (Figures 6B and 6C). Although memory T cells showed a low MFI of pSTAT4 with IL-12 stimulation alone, antigen re-stimulation substantially increased phosphorylation of STAT4, suggesting that both naive and memory $CD8^+$ T cells are similarly shielded from IL-12 signaling without prior antigen (re-)stimulation (Figure S6A). Culturing high- and low-avidity stimulated T cells in the presence or absence of IL-12, we found evidence of differential integration of inflammatory signals, recapitulating the phenotype observed *in vivo*: IL-12 signaling increased CD62L expression measured by MFI in high-avidity T cells (Figures 6D and S6B). In contrast, CD62L expression was diminished in low-avidity T cells after IL-12 stimulation.

Confident that we could model avidity-dependent integration of inflammatory signals *in vitro*, we stimulated T cells with high- or low-avidity peptides, followed by IL-12, and performed CUT&RUN to determine STAT4 binding (Figures 6E, 6F, and S6C). To compare STAT4 genomic binding in $CD8^+$ T cells and NK cells, we performed a comparative motif enrichment analysis. We found that, as observed for NK cells, strong antigen signaling redirected STAT4 away from binding sites containing STAT, RUNX, and ETS toward AP-1 motifs in $CD8^+$ T cells (Figures 6F–6H and S6D). Similar to NK cells, genomic binding of c-Jun was dependent on antigen signaling and was markedly enhanced in T cells stimulated with high-avidity peptide (Figure 6I). Furthermore, $CD8^+$ T cells and NK cells shared genomic sites with increased c-Jun binding, dependent on antigen (Figures 6J and 6K). These data suggest that, in cytotoxic lymphocytes, conserved and stepwise AP-1/STAT4 cooperation regulates their adaptive potential.

Altogether, our data suggest that sufficient antigen-receptor signaling must occur prior to cytokine signaling to drive an optimal adaptive fate in cytotoxic lymphocytes. This stepwise integration is mediated through antigen-strength-dependent STAT/AP-1 cooperation, a feature conserved across lymphocytes, whereby STAT4 is redirected away from STAT, RUNX, and ETS motifs (Figure 6L).

DISCUSSION

The immune system counters pathogen invasion by fulfilling two critical tasks: (1) it must rapidly contain the pathogen and protect the host through a primary response and (2) it must select the best-equipped cells for memory formation in preparation for a more robust secondary response against re-infection. In the midst of a primary response against a pathogen, the immune system cannot afford to be too selective, as even cells with low avidity against a quickly replicating pathogen are preferable to cells that do not recognize the pathogen at all. However, for memory generation, amplifying the number of immune cells with high avidity for the pathogen is desirable.

In our study, we find that the stepwise integration of antigen-receptor and inflammatory cytokine signaling acts to optimize both tasks highlighted above. Whereas immune cells receiving no or inadequate antigen-receptor signaling are driven into a terminal effector fate by inflammatory cytokines during the antiviral response, enhanced memory formation of high-avidity cells

log_2 fold change that increase in binding upon strong antigen compared with weak antigen. Triangle shape indicates peaks above the *y* axis limit ($n = 2$, one experiment).

(F) Tracks of STAT4 CUT&RUN at the *Batf* locus in NK cells and $CD8^+$ T cells given the indicated stimulations.

(G) Scatterplot of log *p* value in hypergeometric optimization of motif enrichment (HOMER) known motif analysis. The top 20% of peaks denoted above, as well as their equivalent in NK cell analysis, were analyzed for enrichment for known motifs in the HOMER database, with STAT4 binding atlas peaks as background. Results were filtered with HOMER's default *p* value threshold (1e−1) and q value threshold of ≤ 0.05. Motifs comparatively enriched for weak/no antigen in the respective datasets were assigned negative values on the respective axes. Colors represent manual categorization of the motifs.

(H) Scatterplot of motif enrichment analysis D statistics from KS tests as described in Figure 2E between NK cells and $CD8^+$ T cells. *AP-1 motif labeled here overlaps three motifs, Atf3, Jun, and Fos::Jun.

(I) Volcano plot of c-Jun CUT&RUN normalized with the flanking method in $CD8^+$ T cells stimulated with strong (N4) versus weak (Q4H7) antigen ($n = 2$, one experiment).

(J) Example tracks from c-Jun CUT&RUN normalized with the flanking method in NK cells and $CD8^+$ T cells in the indicated conditions. Black box: $p < 0.05$.

(K) Scatterplot of c-Jun differential binding dependent on antigen stimulation for $CD8^+$ T cells and NK cells.

(L) Schematic: AP-1/STAT cooperation underlies antigen-dependent differential integration of inflammatory cytokine signaling in innate and adaptive lymphocytes to promote an adaptive/memory fate.

Data in (A)–(D) are representative of two experiments. Error bars represent SEM. Significances were calculated using paired *t* test (same biological replicates). $^{****}p < 0.0001$, $^{***}p < 0.001$, $^{**}p < 0.01$, $^{*}p < 0.05$.

See also Figure S6.

Please cite this article in press as: Grassmann et al., Stepwise epigenetic signal integration drives adaptive programming of cytotoxic lymphocytes, Immunity (2026), https://doi.org/10.1016/j.immuni.2026.01.004

requires adequate antigen-receptor signals prior to encountering inflammation. Previous studies have shown that low-avidity T cells are capable of effector generation[34] and, in fact, generate effector cells earlier than high-avidity T cells,[35] which receive prolonged TCR signaling and stronger interactions with antigen-presenting dendritic cells (DCs). Our study suggests an alternative or additional mechanism, by which the immune system may promote early effector differentiation of low-avidity T cells and NK cells: inflammatory cytokines promote a terminal effector fate in ''suboptimal'' cells, while preferentially selecting high-avidity immune cells for adaptive responses. Fittingly, DCs are the main source of IL-12 during infection[36,37] and could thereby directly govern this fate decision by providing both antigen and cytokine signals.

Previous studies have established that IFN signaling can suppress the proliferative capacity of naive CD8$^+$ T cells,[38,39] while IFN shortly before or after antigen signaling can promote adaptive responses.[40] The proposed mechanism for this effect is a direct inhibitory effect of IFN on cell proliferation, although this mechanism has not been fully established. Another proposed mechanism is that antigen-receptor signaling suppresses STAT1 while promoting STAT4 activation.[41] In contrast to these models, here we propose that STAT4 activation by IL-12 impairs adaptive responses of NK cells via an epigenetic mechanism; however, if the NK cell first receives an antigen signal, STAT4 is redirected to instead promote an adaptive program. Future studies will shed light on how STAT1 and STAT4 shape immune cell differentiation. An additional open question is how antigen and IL-12 signaling shape the integration of subsequent signals. Prior studies in T cells have suggested that regulation of IL-2 signaling via IL-12 could contribute to the pro-proliferative effect of IL-12 in T cells.[42,43] Considering the epigenetic regulation of *Il2ra* and STAT5 in our data, this represents a likely downstream mechanism of antigen-dependent STAT4 redirection, the mechanism proposed in our study.

Future studies will define how the requirement for sequential signal integration shapes immune responses in different contexts. The steady-state expression of the IL-12 receptor by NK cells suggests that this mechanism may inherently limit their adaptive potential. It will also be important to understand what occurs when antigen recognition is not followed by inflammatory cytokine signals. Continuous antigen exposure drives exhaustion in both NK cells[44] and CD8$^+$ T cells,[45] but it remains unresolved whether exhaustion arises primarily from excessive antigen stimulation itself or from a mismatch between antigenic and cytokine cues.[46]

Although antigen-receptor signaling represents a main activator of AP-1 in lymphocytes, it is possible that additional stimuli can sufficiently activate AP-1 to redirect STAT4 genomic binding and facilitate adaptive programming. An obvious candidate is IL-18, which is often used together with IL-12 and IL-15 to generate adaptive-like NK cells *in vitro*.[47] Indeed, IL-18 has been shown to activate downstream AP-1.[48,49] Whether IL-18 drives similar or distinct AP-1 activation compared with activating receptors remains to be determined.

Interactions of STAT and AP-1 TFs have been proposed and observed in various immunological and non-immunological cell types. However, the main STAT TF found to co-operate with AP-1 is STAT3: an AP-1/STAT3 cooperation has been found to regulate the inflammatory memory of epithelial cells[50] and influence the malignant potential of cancer.[51] In CD8$^+$ T cells, STAT3 has been found to bind to genomic regions harboring AP-1, RUNX, and ETS motifs,[52] and the same motifs we identify here to be bound by STAT4. AP-1, ETS, and RUNX TFs have been shown to affect CD8$^+$ T cell[53–55] and NK cell differentiation.[56–58] A recent study proposed STAT4-AP1 cooperation as a requirement for mediating the canonical genomic binding of STAT4 in general.[59] We observe that antigen signaling directs STAT4 away from RUNX and ETS sites and instead promotes STAT/AP-1 cooperation. Our findings suggest an additional layer of complexity, whereby antigen signaling affects the degree to which inflammatory cytokine signaling interacts with distinct TF networks to shape immune cell differentiation.

Beyond infection, our proposed signal integration model could prove crucial in other diseases, such as autoimmunity and cancer.[60,61] In autoimmunity, it has been an outstanding question why inflammatory cytokines can have both protective and detrimental roles.[62] Our study offers a possible explanation. Autoimmunity can be elicited by T cells with low avidity toward self-peptides that escape negative selection and become activated during inflammation or infection.[63] We suggest that STAT4 may act as a negative regulator for adaptive programming of low-avidity T cells, and once autoimmunity has been established, inflammatory cytokines could then promote the expansion of these autoreactive cells.

In cancer, priming of tumor-reactive T cells in lymph nodes is characterized by decreased cytokine signaling compared with priming during infection.[64] At the same time, different tumors vary substantially in the amount of local immune activation, and immunologically ''hot'' tumors respond better to treatments such as immune checkpoint blockade.[65] Our study suggests that a lack of proinflammatory cytokines during priming in tumor-draining lymph nodes may have distinct effects on high- versus low-avidity T cells. Whereas high-avidity T cells will remain below their potential for mounting adaptive responses in the absence of inflammation, low-avidity T cells may, in contrast, be protected from inflammation-induced terminal differentiation. Because high-avidity T cells are often exhausted in tumor settings,[66] the targeting of low-avidity T cells may represent a promising strategy for cancer immunotherapy.

In conclusion, our work highlights a shared molecular mechanism underlying innate and adaptive lymphocyte differentiation, prompting questions about optimal lymphocyte engineering, the context-dependent role of cytokines, and the relationship between the innate and adaptive immune systems.

Limitations of the study

Our study has limitations that will be addressed in future experiments. First, whether a stepwise signal integration mechanism occurs in human NK cells and T cells remains to be investigated. In human NK cells, IL-12 activates STAT5 in addition to STAT4,[67] which may impact antigen-dependent integration of IL-12 signals. Second, intersection of additional synergistic signals (e.g., mechanistic target of rapamycin [mTOR]-related pathways[67]) upstream of the epigenetic mechanisms found in our study will be investigated in the future. Lastly, the relevance of

the observed mechanism of AP-1/STAT4 collaboration for adaptive responses in additional infectious diseases and disease contexts, as well as for vaccination strategies, will be investigated.

RESOURCE AVAILABILITY

Lead contact

Requests for further information, resources, and reagents should be directed to, and will be fulfilled by, the lead contact, Joseph C. Sun (sunj@mskcc.org).

Materials availability

All resources are available upon request to the lead contact.

Data and code availability

Sequencing data have been deposited on GEO and are publicly available from the date of publication. Accession numbers are listed in the key resources table. Software used for coding is listed in the key resources table. This paper did not generate new code. Any additional information required to reanalyze the data reported in this paper is available from the lead contact upon request.

ACKNOWLEDGMENTS

We thank past and present members of the Sun lab for helpful discussions and support, and Dr. Andri Lemarquis, Dr. Sasha Rudensky, Dr. Andrea Schietinger, and Dr. Kilian Schober for input and/or critically reading the manuscript. We further thank Dr. Christina Leslie and Wilfred Wong for help with analysis of CUT&RUN data. Sequencing was performed by the Integrated Genomics Operation Core, which is funded by the NCI Cancer Center Support Grant (CCSG, P30 CA08748), Cycle for Survival, and the Marie-Josée and Henry R. Kravis Center for Molecular Oncology. S.G. is the recipient of a CRI/Donald J. Gogel postdoctoral fellowship (CRI award CR13934) and was supported by the Deutsche Forschungsgemeinschaft (DFG, award number GR5503/1-1) and the NIAID (NIH) under award number K99AI180360. A.M.M. was supported by the CRI as a CRI/Amgen fellow. M.O. was supported by the NIH T32 predoctoral training grant (T32 AI134632-05) and the NIH F31 Ruth L. Kirschstein predoctoral fellowship from the National Institute of Allergy and Infectious Diseases (F31AI178958). S.X.F. was supported by a Medical Scientist Training Program grant from the National Institute of General Medical Sciences of the National Institutes of Health under award number T32GM152349 to the Weill Cornell/Rockefeller/Sloan Kettering Tri-Institutional MD-PhD Program. D.H.B. was supported by SFB-TRR 338/1 2021-452881907 (project A01) and SFB-1371 395357507 (project P04). J.C.S. was supported by the Ludwig Center for Cancer Immunotherapy, the American Cancer Society, the Burroughs Wellcome Fund, and the NIH (AI100874, AI130043, AI155558, and P30CA008748).

AUTHOR CONTRIBUTIONS

S.G. and J.C.S designed the study and wrote the manuscript. S.G., E.K.S., I.B.J., A.M.M., J.-B.L., S.X.F., and M.O. performed experiments. E.K.S. and H.K. performed computational analyses. A.S. and D.H.B. provided crucial materials and input for retrogenic mouse generation. L.D. provided MVAΔE5R-OVA and related expertise for recall experiments. K.C.H. and C.M.L. provided crucial insights into experiment design and data analysis.

DECLARATION OF INTERESTS

The authors declare no competing interests.

STAR★METHODS

Detailed methods are provided in the online version of this paper and include the following:

- KEY RESOURCES TABLE
- EXPERIMENTAL MODEL AND STUDY PARTICIPANT DETAILS
  - Mice
  - MCMV virus preparation
- METHOD DETAILS
  - Mixed bone-marrow chimeras
  - Infections of *Nr4a1*-GFP mice and mixed bone marrow chimera
  - Isolation of mouse NK cells and flow cytometry
  - Cell culture for *in vitro* experiments
  - *In vitro* receptor and cytokine stimulation for sequencing of NK cells
  - CTV dilution and proliferation assay
  - Generation of retrogenic mice
  - $CD8^+$ T cell peptide stimulation
  - T cell transfer and Listeria infection
  - MVAΔE5R-OVA infection
  - Single-cell RNA-sequencing and analysis
  - RNA-sequencing
  - ATAC-sequencing
  - Transcription factor CUT&RUN
  - RNA-seq, ChIP-seq, CUT&RUN, and ATAC-seq data processing
  - Motif analysis
  - Downstream analyses of RNA-seq and ATAC-seq
  - Visualization of RNA-seq, CUT&RUN and ATAC-seq

SUPPLEMENTAL INFORMATION

Supplemental information can be found online at https://doi.org/10.1016/j.immuni.2026.01.004.

Received: May 2, 2025
Revised: September 17, 2025
Accepted: January 5, 2026

REFERENCES

1. Chung, H.K., McDonald, B., and Kaech, S.M. (2021). The architectural design of CD8+ T cell responses in acute and chronic infection: Parallel structures with divergent fates. J. Exp. Med. *218*, e20201730. https://doi.org/10.1084/jem.20201730.
2. Adams, N.M., Grassmann, S., and Sun, J.C. (2020). Clonal expansion of innate and adaptive lymphocytes. Nat. Rev. Immunol. *20*, 694–707. https://doi.org/10.1038/s41577-020-0307-4.
3. Chang, J.T., Wherry, E.J., and Goldrath, A.W. (2014). Molecular regulation of effector and memory T cell differentiation. Nat. Immunol. *15*, 1104–1115. https://doi.org/10.1038/ni.3031.
4. Kaech, S.M., and Cui, W. (2012). Transcriptional control of effector and memory CD8+ T cell differentiation. Nat. Rev. Immunol. *12*, 749–761. https://doi.org/10.1038/nri3307.
5. Busch, D.H., and Pamer, E.G. (1999). T Cell Affinity Maturation by Selective Expansion during Infection. J. Exp. Med. *189*, 701–710. https://doi.org/10.1084/jem.189.4.701.
6. Joshi, N.S., Cui, W., Chandele, A., Lee, H.K., Urso, D.R., Hagman, J., Gapin, L., and Kaech, S.M. (2007). Inflammation directs memory precursor and short-lived effector CD8(+) T cell fates via the graded expression of T-bet transcription factor. Immunity *27*, 281–295. https://doi.org/10.1016/j.immuni.2007.07.010.
7. Pearce, E.L., and Shen, H. (2007). Generation of CD8 T cell memory is regulated by IL-12. J. Immunol. *179*, 2074–2081. https://doi.org/10.4049/jimmunol.179.4.2074.
8. Xiao, Z., Casey, K.A., Jameson, S.C., Curtsinger, J.M., and Mescher, M.F. (2009). Programming for CD8 T cell memory development requires IL-12 or type I IFN. J. Immunol. *182*, 2786–2794. https://doi.org/10.4049/jimmunol.0803484.
9. Keppler, S.J., Theil, K., Vucikuja, S., and Aichele, P. (2009). Effector T-cell differentiation during viral and bacterial infections: Role of direct IL-12 signals for cell fate decision of CD8(+) T cells. Eur. J. Immunol. *39*, 1774–1783. https://doi.org/10.1002/eji.200839093.

10. Sun, J.C., Beilke, J.N., and Lanier, L.L. (2009). Adaptive immune features of natural killer cells. Nature *457*, 557–561. https://doi.org/10.1038/nature07665.

11. Mujal, A.M., Delconte, R.B., and Sun, J.C. (2021). Natural Killer Cells: From Innate to Adaptive Features. Annu. Rev. Immunol. *39*, 417–447. https://doi.org/10.1146/annurev-immunol-101819-074948.

12. Dokun, A.O., Kim, S., Smith, H.R., Kang, H.S., Chu, D.T., and Yokoyama, W.M. (2001). Specific and nonspecific NK cell activation during virus infection. Nat. Immunol. *2*, 951–956. https://doi.org/10.1038/ni714.

13. Brown, M.G., Dokun, A.O., Heusel, J.W., Smith, H.R.C., Beckman, D.L., Blattenberger, E.A., Dubbelde, C.E., Stone, L.R., Scalzo, A.A., and Yokoyama, W.M. (2001). Vital Involvement of a Natural Killer Cell Activation Receptor in Resistance to Viral Infection. Science *292*, 934–937. https://doi.org/10.1126/science.1060042.

14. Grassmann, S., Pachmayr, L.O., Leube, J., Mihatsch, L., Andrae, I., Flommersfeld, S., Oduro, J., Cicin-Sain, L., Schiemann, M., Flossdorf, M., et al. (2019). Distinct Surface Expression of Activating Receptor Ly49H Drives Differential Expansion of NK Cell Clones upon Murine Cytomegalovirus Infection. Immunity *50*, 1391–1400.e4. https://doi.org/10.1016/j.immuni.2019.04.015.

15. Adams, N.M., Geary, C.D., Santosa, E.K., Lumaquin, D., Le Luduec, J.B., Sottile, R., van der Ploeg, K., Hsu, J., Whitlock, B.M., Jackson, B.T., et al. (2019). Cytomegalovirus Infection Drives Avidity Selection of Natural Killer Cells. Immunity *50*, 1381–1390.e5. https://doi.org/10.1016/j.immuni.2019.04.009.

16. Wiedemann, G.M., Grassmann, S., Lau, C.M., Rapp, M., Villarino, A.V., Friedrich, C., Gasteiger, G., O'Shea, J.J., and Sun, J.C. (2020). Divergent Role for STAT5 in the Adaptive Responses of Natural Killer Cells. Cell Rep. *33*, 108498. https://doi.org/10.1016/j.celrep.2020.108498.

17. Sun, J.C., Madera, S., Bezman, N.A., Beilke, J.N., Kaplan, M.H., and Lanier, L.L. (2012). Proinflammatory cytokine signaling required for the generation of natural killer cell memory. J. Exp. Med. *209*, 947–954. https://doi.org/10.1084/jem.20111760.

18. Madera, S., Rapp, M., Firth, M.A., Beilke, J.N., Lanier, L.L., and Sun, J.C. (2016). Type I IFN promotes NK cell expansion during viral infection by protecting NK cells against fratricide. J. Exp. Med. *213*, 225–233. https://doi.org/10.1084/jem.20150712.

19. Lanier, L.L. (1998). NK cell receptors. Annu. Rev. Immunol. *16*, 359–393. https://doi.org/10.1146/annurev.immunol.16.1.359.

20. Pegram, H.J., Andrews, D.M., Smyth, M.J., Darcy, P.K., and Kershaw, M.H. (2011). Activating and inhibitory receptors of natural killer cells. Immunol. Cell Biol. *89*, 216–224. https://doi.org/10.1038/icb.2010.78.

21. Wiedemann, G.M., Santosa, E.K., Grassmann, S., Sheppard, S., Le Luduec, J.-B., Adams, N.M., Dang, C., Hsu, K.C., Sun, J.C., and Lau, C.M. (2021). Deconvoluting global cytokine signaling networks in natural killer cells. Nat. Immunol. *22*, 627–638. https://doi.org/10.1038/s41590-021-00909-1.

22. Liu, Z.G., Smith, S.W., McLaughlin, K.A., Schwartz, L.M., and Osborne, B.A. (1994). Apoptotic signals delivered through the T-cell receptor of a T-cell hybrid require the immediate–early gene nur77. Nature *367*, 281–284. https://doi.org/10.1038/367281a0.

23. Moran, A.E., Holzapfel, K.L., Xing, Y., Cunningham, N.R., Maltzman, J.S., Punt, J., and Hogquist, K.A. (2011). T cell receptor signal strength in Treg and iNKT cell development demonstrated by a novel fluorescent reporter mouse. J. Exp. Med. *208*, 1279–1289. https://doi.org/10.1084/jem.20110308.

24. Dong, H., Adams, N.M., Xu, Y., Cao, J., Allan, D.S.J., Carlyle, J.R., Chen, X., Sun, J.C., and Glimcher, L.H. (2019). The IRE1 endoplasmic reticulum stress sensor activates natural killer cell immunity in part by regulating c-Myc. Nat. Immunol. *20*, 865–878. https://doi.org/10.1038/s41590-019-0388-z.

25. Santosa, E.K., Kim, H., Rückert, T., Le Luduec, J.-B., Abbasi, A.J., Wingert, C.K., Peters, L., Frost, J.N., Hsu, K.C., Romagnani, C., and Sun, J.C. (2023). Control of nutrient uptake by IRF4 orchestrates innate immune memory. Nat. Immunol. *24*, 1685–1697. https://doi.org/10.1038/s41590-023-01620-z.

26. Vierbuchen, T., Ling, E., Cowley, C.J., Couch, C.H., Wang, X., Harmin, D.A., Roberts, C.W.M., and Greenberg, M.E. (2017). AP-1 Transcription Factors and the BAF Complex Mediate Signal-Dependent Enhancer Selection. Mol. Cell *68*, 1067–1082.e12. https://doi.org/10.1016/j.molcel.2017.11.026.

27. Mujal, A.M., Owyong, M., Santosa, E.K., Sauter, J.C., Grassmann, S., Pedde, A.-M., Meiser, P., Wingert, C.K., Pujol, M., Buchholz, V.R., et al. (2025). Splenic TNF-α signaling potentiates the innate-to-adaptive transition of antiviral NK cells. Immunity *58*, 585–600.e6. https://doi.org/10.1016/j.immuni.2025.02.012.

28. Lau, C.M., Adams, N.M., Geary, C.D., Weizman, O.E., Rapp, M., Pritykin, Y., Leslie, C.S., and Sun, J.C. (2018). Epigenetic control of innate and adaptive immune memory. Nat. Immunol. *19*, 963–972. https://doi.org/10.1038/s41590-018-0176-1.

29. Li, Q., Eppolito, C., Odunsi, K., and Shrikant, P.A. (2006). IL-12-Programmed Long-Term CD8+ T Cell Responses Require STAT41. J. Immunol. *177*, 7618–7625. https://doi.org/10.4049/jimmunol.177.11.7618.

30. Straub, A., Grassmann, S., Jarosch, S., Richter, L., Hilgendorf, P., Hammel, M., Wagner, K.I., Buchholz, V.R., Schober, K., and Busch, D.H. (2023). Recruitment of epitope-specific T cell clones with a low-avidity threshold supports efficacy against mutational escape upon re-infection. Immunity *56*, 1269–1284.e6. https://doi.org/10.1016/j.immuni.2023.04.010.

31. Yang, N., Wang, Y., Dai, P., Li, T., Zierhut, C., Tan, A., Zhang, T., Xiang, J.Z., Ordureau, A., Funabiki, H., et al. (2023). Vaccinia E5 is a major inhibitor of the DNA sensor cGAS. Nat. Commun. *14*, 2898. https://doi.org/10.1038/s41467-023-38514-5.

32. Pais Ferreira, D., Silva, J.G., Wyss, T., Fuertes Marraco, S.A., Scarpellino, L., Charmoy, M., Maas, R., Siddiqui, I., Tang, L., Joyce, J.A., et al. (2020). Central memory CD8+ T cells derive from stem-like Tcf7hi effector cells in the absence of cytotoxic differentiation. Immunity *53*, 985–1000.e11. https://doi.org/10.1016/j.immuni.2020.09.005.

33. Grassmann, S., Mihatsch, L., Mir, J., Kazeroonian, A., Rahimi, R., Flommersfeld, S., Schober, K., Hensel, I., Leube, J., Pachmayr, L.O., et al. (2020). Early emergence of T central memory precursors programs clonal dominance during chronic viral infection. Nat. Immunol. *21*, 1563–1573. https://doi.org/10.1038/s41590-020-00807-y.

34. Zehn, D., Lee, S.Y., and Bevan, M.J. (2009). Complete but curtailed T-cell response to very low-affinity antigen. Nature *458*, 211–214. https://doi.org/10.1038/nature07657.

35. Ozga, A.J., Moalli, F., Abe, J., Swoger, J., Sharpe, J., Zehn, D., Kreutzfeldt, M., Merkler, D., Ripoll, J., and Stein, J.V. (2016). pMHC affinity controls duration of CD8+ T cell-DC interactions and imprints timing of effector differentiation versus expansion. J. Exp. Med. *213*, 2811–2829. https://doi.org/10.1084/jem.20160206.

36. Heufler, C., Koch, F., Stanzl, U., Topar, G., Wysocka, M., Trinchieri, G., Enk, A., Steinman, R.M., Romani, N., and Schuler, G. (1996). Interleukin-12 is produced by dendritic cells and mediates T helper 1 development as well as interferon-gamma production by T helper 1 cells. Eur. J. Immunol. *26*, 659–668. https://doi.org/10.1002/eji.1830260323.

37. Henry, C.J., Ornelles, D.A., Mitchell, L.M., Brzoza-Lewis, K.L., and Hiltbold, E.M. (2008). IL-12 produced by dendritic cells augments CD8+ T cell activation through the production of the chemokines CCL1 and CCL17. J. Immunol. *181*, 8576–8584. https://doi.org/10.4049/jimmunol.181.12.8576.

38. Marshall, H.D., Urban, S.L., and Welsh, R.M. (2011). Virus-induced transient immune suppression and the inhibition of T cell proliferation by type I interferon. J. Virol. *85*, 5929–5939. https://doi.org/10.1128/jvi.02516-10.

39. Broomfield, B.J., Tan, C.W., Qin, R.Z., Abberger, H., Duckworth, B.C., Alvarado, C., Dalit, L., Lee, C.L., Shandre Mugan, R., Mazrad, Z.A.I., et al. (2025). Transient inhibition of type I interferon enhances CD8+ T cell stemness and vaccine protection. J. Exp. Med. *222*, e20241148. https://doi.org/10.1084/jem.20241148.

40. Le Bon, A., Durand, V., Kamphuis, E., Thompson, C., Bulfone-Paus, S., Rossmann, C., Kalinke, U., and Tough, D.F. (2006). Direct stimulation of T cells by type I IFN enhances the CD8+ T cell response during cross-priming. J. Immunol. *176*, 4682–4689. https://doi.org/10.4049/jimmunol.176.8.4682.

41. Gil, M.P., Ploquin, M.J.Y., Watford, W.T., Lee, S.H., Kim, K., Wang, X., Kanno, Y., O'Shea, J.J., and Biron, C.A. (2012). Regulating type 1 IFN effects in CD8 T cells during viral infections: changing STAT4 and STAT1 expression for function. Blood *120*, 3718–3728. https://doi.org/10.1182/blood-2012-05-428672.

42. Starbeck-Miller, G.R., Xue, H.H., and Harty, J.T. (2014). IL-12 and type I interferon prolong the division of activated CD8 T cells by maintaining high-affinity IL-2 signaling in vivo. J. Exp. Med. *211*, 105–120. https://doi.org/10.1084/jem.20130901.

43. Valenzuela, J., Schmidt, C., and Mescher, M. (2002). The roles of IL-12 in providing a third signal for clonal expansion of naive CD8 T cells. J. Immunol. *169*, 6842–6849. https://doi.org/10.4049/jimmunol.169.12.6842.

44. Myers, J.A., Schirm, D., Bendzick, L., Hopps, R., Selleck, C., Hinderlie, P., Felices, M., and Miller, J.S. (2022). Balanced engagement of activating and inhibitory receptors mitigates human NK cell exhaustion. JCI Insight *7*, e150079. https://doi.org/10.1172/jci.insight.150079.

45. Mueller, S.N., and Ahmed, R. (2009). High antigen levels are the cause of T cell exhaustion during chronic viral infection. Proc. Natl. Acad. Sci. USA *106*, 8623–8628. https://doi.org/10.1073/pnas.0809818106.

46. Baessler, A., and Vignali, D.A.A. (2024). T Cell Exhaustion. Annu. Rev. Immunol. *42*, 179–206. https://doi.org/10.1146/annurev-immunol-090222-110914.

47. Cooper, M.A., Elliott, J.M., Keyel, P.A., Yang, L., Carrero, J.A., and Yokoyama, W.M. (2009). Cytokine-induced memory-like natural killer cells. Proc. Natl. Acad. Sci. USA *106*, 1915–1919. https://doi.org/10.1073/pnas.0813192106.

48. Lee, J.K., Kim, S.H., Lewis, E.C., Azam, T., Reznikov, L.L., and Dinarello, C.A. (2004). Differences in signaling pathways by IL-1beta and IL-18. Proc. Natl. Acad. Sci. USA *101*, 8815–8820. https://doi.org/10.1073/pnas.0402800101.

49. Nakahira, M., Ahn, H.-J., Park, W.-R., Gao, P., Tomura, M., Park, C.-S., Hamaoka, T., Ohta, T., Kurimoto, M., and Fujiwara, H. (2002). Synergy of IL-12 and IL-18 for IFN-γ Gene Expression: IL-12-Induced STAT4 Contributes to IFN-γ Promoter Activation by Up-Regulating the Binding Activity of IL-18-Induced Activator Protein 11. J. Immunol. *168*, 1146–1153. https://doi.org/10.4049/jimmunol.168.3.1146.

50. Larsen, S.B., Cowley, C.J., Sajjath, S.M., Barrows, D., Yang, Y., Carroll, T.S., and Fuchs, E. (2021). Establishment, maintenance, and recall of inflammatory memory. Cell Stem Cell *28*, 1758–1774.e8. https://doi.org/10.1016/j.stem.2021.07.001.

51. He, L., Pratt, H., Gao, M., Wei, F., Weng, Z., and Struhl, K. (2021). YAP and TAZ are transcriptional co-activators of AP-1 proteins and STAT3 during breast cellular transformation. eLife *10*, e67312. https://doi.org/10.7554/eLife.67312.

52. Sun, Q., Zhao, X., Li, R., Liu, D., Pan, B., Xie, B., Chi, X., Cai, D., Wei, P., Xu, W., et al. (2023). STAT3 regulates CD8+ T cell differentiation and functions in cancer and acute infection. J. Exp. Med. *220*, e20220686. https://doi.org/10.1084/jem.20220686.

53. Ataide, M.A., Komander, K., Knöpper, K., Peters, A.E., Wu, H., Eickhoff, S., Gogishvili, T., Weber, J., Grafen, A., Kallies, A., et al. (2020). BATF3 programs CD8+ T cell memory. Nat. Immunol. *21*, 1397–1407. https://doi.org/10.1038/s41590-020-0786-2.

54. Tsuda, S.M., Diao, H., Getzler, A., Milner, J., Goldrath, A.W., Crotty, S., and Pipkin, M.E. (2021). Ets1 governs the differential formation of circulating and tissue-resident memory CD8 T cells. J. Immunol. *206*, 98.56. https://doi.org/10.4049/jimmunol.206.Supp.98.56.

55. Woolf, E., Xiao, C., Fainaru, O., Lotem, J., Rosen, D., Negreanu, V., Bernstein, Y., Goldenberg, D., Brenner, O., Berke, G., et al. (2003). Runx3 and Runx1 are required for CD8 T cell development during thymopoiesis. Proc. Natl. Acad. Sci. USA *100*, 7731–7736. https://doi.org/10.1073/pnas.1232420100.

56. Rückert, T., Lareau, C.A., Mashreghi, M.-F., Ludwig, L.S., and Romagnani, C. (2022). Clonal expansion and epigenetic inheritance of long-lasting NK cell memory. Nat. Immunol. *23*, 1551–1563. https://doi.org/10.1038/s41590-022-01327-7.

57. Rapp, M., Lau, C.M., Adams, N.M., Weizman, O.E., O'Sullivan, T.E., Geary, C.D., and Sun, J.C. (2017). Core-binding factor β and Runx transcription factors promote adaptive natural killer cell responses. Sci. Immunol. *2*, eaan3796. https://doi.org/10.1126/sciimmunol.aan3796.

58. Ramirez, K., Chandler, K.J., Spaulding, C., Zandi, S., Sigvardsson, M., Graves, B.J., and Kee, B.L. (2012). Gene deregulation and chronic activation in natural killer cells deficient in the transcription factor ETS1. Immunity *36*, 921–932. https://doi.org/10.1016/j.immuni.2012.04.006.

59. Philips, R.L., Liao, Y.C., Lau, C.M., Morrison, T.A., Jiang, K., Hutchinson, A., Shayne, J., Yao, C., Sun, J.C., Hickman, H.D., et al. (2025). An activating Stat1 mutant disrupts normal STAT4 innate lymphocyte programs during viral infection. Sci. Immunol. *10*, eado5986. https://doi.org/10.1126/sciimmunol.ado5986.

60. Crow, M.K., Olferiev, M., and Kirou, K.A. (2019). Type I Interferons in Autoimmune Disease. Annu. Rev. Pathol.: Mech. Dis. *14*, 369–393. https://doi.org/10.1146/annurev-pathol-020117-043952.

61. Propper, D.J., and Balkwill, F.R. (2022). Harnessing cytokines and chemokines for cancer therapy. Nat. Rev. Clin. Oncol. *19*, 237–253. https://doi.org/10.1038/s41571-021-00588-9.

62. O'Shea, J.J., Ma, A., and Lipsky, P. (2002). Cytokines and autoimmunity. Nat. Rev. Immunol. *2*, 37–45. https://doi.org/10.1038/nri702.

63. Enouz, S., Carrié, L., Merkler, D., Bevan, M.J., and Zehn, D. (2012). Autoreactive T cells bypass negative selection and respond to self-antigen stimulation during infection. J. Exp. Med. *209*, 1769–1779. https://doi.org/10.1084/jem.20120905.

64. Prokhnevska, N., Cardenas, M.A., Valanparambil, R.M., Sobierajska, E., Barwick, B.G., Jansen, C., Reyes Moon, A., Gregorova, P., delBalzo, L., Greenwald, R., et al. (2023). CD8+ T cell activation in cancer comprises an initial activation phase in lymph nodes followed by effector differentiation within the tumor. Immunity *56*, 107–124.e5. https://doi.org/10.1016/j.immuni.2022.12.002.

65. Zhang, J., Huang, D., Saw, P.E., and Song, E. (2022). Turning cold tumors hot: from molecular mechanisms to clinical applications. Trends Immunol. *43*, 523–545. https://doi.org/10.1016/j.it.2022.04.010.

66. Shakiba, M., Zumbo, P., Espinosa-Carrasco, G., Menocal, L., Dündar, F., Carson, S.E., Bruno, E.M., Sanchez-Rivera, F.J., Lowe, S.W., Camara, S., et al. (2021). TCR signal strength defines distinct mechanisms of T cell dysfunction and cancer evasion. J. Exp. Med. *219*, e20201966. https://doi.org/10.1084/jem.20201966.

67. Shemesh, A., Pickering, H., Roybal, K.T., and Lanier, L.L. (2022). Differential IL-12 signaling induces human natural killer cell activating receptor-mediated ligand-specific expansion. J. Exp. Med. *219*, e20212434. https://doi.org/10.1084/jem.20212434.

68. Galili, T. (2015). dendextend: an R package for visualizing, adjusting and comparing trees of hierarchical clustering. Bioinformatics *31*, 3718–3720. https://doi.org/10.1093/bioinformatics/btv428.

69. Gu, Z., Gu, L., Eils, R., Schlesner, M., and Brors, B. (2014). circlize implements and enhances circular visualization in R. Bioinformatics *30*, 2811–2812. https://doi.org/10.1093/bioinformatics/btu393.

70. Gu, Z. (2022). Complex heatmap visualization. Imeta *1*, e43. https://doi.org/10.1002/imt2.43.

71. Ritchie, M.E., Phipson, B., Wu, D., Hu, Y., Law, C.W., Shi, W., and Smyth, G.K. (2015). limma powers differential expression analyses for RNA-sequencing and microarray studies. Nucleic Acids Res. *43*, e47. https://doi.org/10.1093/nar/gkv007.

72. Love, M.I., Huber, W., and Anders, S. (2014). Moderated estimation of fold change and dispersion for RNA-seq data with DESeq2. Genome Biol. *15*, 550. https://doi.org/10.1186/s13059-014-0550-8.

73. Lawrence, M., Huber, W., Pagès, H., Aboyoun, P., Carlson, M., Gentleman, R., Morgan, M.T., and Carey, V.J. (2013). Software for computing and annotating genomic ranges. PLoS Comput. Biol. *9*, e1003118. https://doi.org/10.1371/journal.pcbi.1003118.

74. Zhu, L.J., Gazin, C., Lawson, N.D., Pagès, H., Lin, S.M., Lapointe, D.S., and Green, M.R. (2010). ChIPpeakAnno: a Bioconductor package to annotate ChIP-seq and ChIP-chip data. BMC Bioinform. *11*, 237. https://doi.org/10.1186/1471-2105-11-237.

75. Huber, W., Carey, V.J., Gentleman, R., Anders, S., Carlson, M., Carvalho, B.S., Bravo, H.C., Davis, S., Gatto, L., Girke, T., et al. (2015). Orchestrating high-throughput genomic analysis with Bioconductor. Nat. Methods *12*, 115–121. https://doi.org/10.1038/nmeth.3252.

76. Lawrence, M., Gentleman, R., and Carey, V. (2009). rtracklayer: an R package for interfacing with genome browsers. Bioinformatics *25*, 1841–1842. https://doi.org/10.1093/bioinformatics/btp328.

77. (2016). ggplot2: Elegant Graphics for Data Analysis (New York: Springer-Verlag).

78. Wickham, H.. stringr: Simple, Consistent Wrappers for Common String Operations. R package version 1.6.0. https://stringr.tidyverse.org.

79. Andrews, S. (2010). FastQC: A Quality Control Tool for High Throughput Sequence Data [Online]. Available online at: http://www.bioinformatics.babraham.ac.uk/projects/fastqc/

80. Bolger, A.M., Lohse, M., and Usadel, B. (2014). Trimmomatic: a flexible trimmer for Illumina sequence data. Bioinformatics *30*, 2114–2120. https://doi.org/10.1093/bioinformatics/btu170.

81. Langmead, B., and Salzberg, S.L. (2012). Fast gapped-read alignment with Bowtie 2. Nat. Methods *9*, 357–359. https://doi.org/10.1038/nmeth.1923.

82. Zhang, Y., Liu, T., Meyer, C.A., Eeckhoute, J., Johnson, D.S., Bernstein, B.E., Nusbaum, C., Myers, R.M., Brown, M., Li, W., and Liu, X.S. (2008). Model-based analysis of ChIP-Seq (MACS). Genome Biol. *9*, R137. https://doi.org/10.1186/gb-2008-9-9-r137.

83. Ramírez, F., Ryan, D.P., Grüning, B., Bhardwaj, V., Kilpert, F., Richter, A.S., Heyne, S., Dündar, F., and Manke, T. (2016). deepTools2: a next generation web server for deep-sequencing data analysis. Nucleic Acids Res. *44*, W160–W165. https://doi.org/10.1093/nar/gkw257.

84. Danecek, P., Bonfield, J.K., Liddle, J., Marshall, J., Ohan, V., Pollard, M.O., Whitwham, A., Keane, T., McCarthy, S.A., Davies, R.M., and Li, H. (2021). Twelve years of SAMtools and BCFtools. GigaScience *10*, giab008. https://doi.org/10.1093/gigascience/giab008.

85. Heinz, S., Benner, C., Spann, N., Bertolino, E., Lin, Y.C., Laslo, P., Cheng, J.X., Murre, C., Singh, H., and Glass, C.K. (2010). Simple combinations of lineage-determining transcription factors prime cis-regulatory elements required for macrophage and B cell identities. Mol. Cell *38*, 576–589. https://doi.org/10.1016/j.molcel.2010.05.004.

86. Mason, L.H., Anderson, S.K., Yokoyama, W.M., Smith, H.R.C., Winkler-Pickett, R., and Ortaldo, J.R. (1996). The Ly-49D Receptor Activates Murine Natural Killer Cells. J. Exp. Med. *184*, 2119–2128. https://doi.org/10.1084/jem.184.6.2119.

87. Buenrostro, J.D., Giresi, P.G., Zaba, L.C., Chang, H.Y., and Greenleaf, W.J. (2013). Transposition of native chromatin for fast and sensitive epigenomic profiling of open chromatin, DNA-binding proteins and nucleosome position. Nat. Methods *10*, 1213–1218. https://doi.org/10.1038/nmeth.2688.

88. Santosa, E.K., Lau, C.M., Sahin, M., Leslie, C.S., and Sun, J.C. (2023). 3D Chromatin Dynamics during Innate and Adaptive Immune Memory Acquisition. Preprint at bioRxiv. https://doi.org/10.1101/2023.01.16.524322.

89. Kim, H., Abbasi, A., Sharrock, J., Santosa, E.K., Sheppard, S., Lau, C.M., Edelson, B.T., and Sun, J.C. (2023). Cutting Edge: STAT4 Promotes Bhlhe40 Induction to Drive Protective IFN-γ from NK Cells during Viral Infection. J. Immunol. *211*, 1469–1474. https://doi.org/10.4049/jimmunol.2300402.

Please cite this article in press as: Grassmann et al., Stepwise epigenetic signal integration drives adaptive programming of cytotoxic lymphocytes, Immunity (2026), https://doi.org/10.1016/j.immuni.2026.01.004

STAR★METHODS

KEY RESOURCES TABLE

REAGENT or RESOURCE	SOURCE	IDENTIFIER
Antibodies		
aCD49b	BD Biosciences	HMa2, Cat. 740250; RRID: AB_3685117
aCD49a	BD Biosciences	Ha31/8, Cat. 741111; RRID: AB_2870703
aCD62L	BD Biosciences	MEL-14, Cat. 612833; RRID: AB_2870155
aNK1.1	BD Biosciences	PK136, Cat. 741926; RRID: AB_2871239
aCD122	eBioscience	M-B1, Cat. 48-1222-82; RRID: AB_2016697
aCD127	Biolegend	A7R34, Cat. 135027; RRID: AB_2563103
aCD69	Biolegend	H1.2F3, Cat. 104530; RRID: AB_2074979
aLy6C	Biolegend	HK1.4, Cat. 128037; RRID: AB_2562630
aKLRG1	Biolegend	2F1/KLRG1, Cat. 138429; RRID: AB_2629749
aCD11b	eBioscience	M1/70, Cat. 58-0112-82; RRID: AB_2811905
aLy49D	Biolegend	4E5, Cat. 138307; RRID: AB_10640823
aDNAM1	Biolegend	1E6, Cat. 128818; RRID: AB_2632823
aCD27	Invitrogen	LG.7F9, Cat. 25-0271-82; RRID: AB_1724035
aLy49H	eBioscience	3D10, Cat. 17-5886-82; RRID: AB_2737633
aCD19	eBioscience	6D5, Cat. 115530; RRID: AB_830707
aTCRb	Biolegend	H57-597, Cat. B131870; RRID: AB_893624
aLy6G	Biolegend	1A8, Cat. 127623; RRID: AB_1877261
aCD25	BD Biosciences	PC61, Cat. 564022; RRID: AB_2722574
aCD8	BD Biosciences	53-6.7, Cat. 748535; RRID: AB_2872946
aCD45.1	BD Biosciences	A20, Cat. 751467; RRID: AB_2875463
aCD127	Biolegend	A7R34, Cat. 135023; RRID: AB_10897948
aPD-1	Biolegend	29F.1A12, Cat. 135220; RRID: AB_2562616
aCD44	Biolegend	IM7, Cat. 103057; RRID: AB_2564214
aVa2	Biolegend	B20.1, Cat. 127805; RRID: AB_2129794
aTCF1	BD Biosciences	S33-966, Cat. 564217; RRID: AB_1134186
aVb5	Biolegend	MR-94, Cat. 139505; RRID: AB_10897800
aCD45.2	Biolegend	104, Cat. 109822; RRID: AB_493731
polyclonal anti-STAT4	ThermoFisher	Cat. 71-4500; RRID: AB_2533985
polyclonal anti-STAT1	Proteintech	Cat. 10144-2-AP; RRID: AB_2286875
polyclonal anti-STAT5b	ThermoFisher	Cat. 71-2500; RRID: AB_2533980
anti-c-JUN	Cell Signaling	Cat. 9165T; RRID: AB_2130165
BioMag Goat Anti-Rat IgG	Qiagen	Cat. 310107
InVivoMAb anti-mouse CD3	BioXcell	17A2, Cat. BE0002; RRID: AB_1107630
InVivoMab Anti-Mouse CD8α	BioXcell	2.43, Cat. BE0061; RRID: AB_1125541
InVivoMab Anti-Mouse CD4	BioXcell	GK1.5, Cat. BE0003-1; RRID: AB_1107636
InVivoMab Anti-Mouse CD19	BioXcell	1D3, Cat. BE0150; RRID: AB_10949187
InVivoMab Anti-Mouse Ly6G	BioXcell	1A8, Cat. BE0075-1; RRID: AB_1107721
Bacterial and virus strains		
MCMV (Smith Strain)	N/A	N/A
Listeria-OVA	Michael Bevan (PI)	N/A
MVAΔE5R-OVA	Liang Deng (PI)	N/A
Chemicals, peptides, and recombinant proteins		
SIINFEKL	Anaspec	Cat. AS-60193-1
SIIQFEHL	Anaspec	Cat. AS-64405

(*Continued on next page*)

Please cite this article in press as: Grassmann et al., Stepwise epigenetic signal integration drives adaptive programming of cytotoxic lymphocytes, Immunity (2026), https://doi.org/10.1016/j.immuni.2026.01.004

Continued

REAGENT or RESOURCE	SOURCE	IDENTIFIER
Recombinant Mouse IL-12	R&D Systems	Cat. 419-ML
Human IL-15, research grade	Miltenyi	Cat. 130-093-955
SR 11302 (Pan AP-1 inhibitor)	Tocris	Cat. 2476
Critical commercial assays		
MinElute PCR Purification Kit	Qiagen	Cat. 28006
KAPA Hyper Prep Kit	Roche/Fisher	Cat. 7962363001
Illumina Tagment DNA TDE1 Enzyme and Buffer Kits	Illumina	Cat. 20034197
NK Cell Isolation Kit	Miltenyi	Cat. 130-115-818
Arcturus PicoPure RNA Isolation Kit	Thermo Fisher	Cat. KIT0204
Quick-RNA Microprep Kit	Zymo Research	Cat. R1051
SMART-Seq v4 Ultra Low Input RNA Kit	Clonetech	Cat. 63488
eBioscience Transcription Factor Staining Buffer Set	Thermo Fisher	Cat. 00-5523-00
NovaSeq 6000 S1 or S4 Reagent Kit	Illumina	Cat. 20028318
pAG-MNase / Spike-in DNA	Cell Signaling	Cat. 40366
Deposited data		
Superseries: GEO: GSE309370		
CUT&RUN: STAT4	This paper	GEO: GSE292293
bulk RNA- and ATAC-seq	This paper	GEO: GSE292377
CUT&RUN: STAT1 STAT5 c-Jun	This paper	GEO: GSE308415
ATAC-seq AP1inhibitor	This paper	GEO: GSE308414
bulk RNA- and ATAC-seq G	This paper	GEO: GSE309245
scRNA-seq	This paper	GEO: GSE292296
Experimental models: Cell lines		
HEK293 cells	ATCC	CRL-1573
Experimental models: Organisms/strains		
C57BL/6J CD45.2	The Jackson Laboratory	Strain# 000664
C57BL/6J CD45.1 (Stem.1)	David T Scadden (PI)	N/A
C57BL/6J CD45.1 × CD45.2	N/A	N/A
Klra8$^{-/-}$	Silvia M Vidal (PI)	N/A
Ncr1-GFP	The Jackson Laboratory	Strain # 022739
Nr4a1-GFP	The Jackson Laboratory	Strain # 016617
IL12rb2$^{-/-}$	The Jackson Laboratory	Strain # 003248
OT-1	The Jackson Laboratory	Strain # 003831
Recombinant DNA		
pEco Plasmid	Addgene	Plasmid #12371
pMP71 (Clone B11)	Straub et al.[30]	B11
pMP71 (Clone E8)	Straub et al.[30]	E8
Software and algorithms		
dendextend	Galili[68]	v1.19.0
circlize	Gu et al.[69]	v0.4.16
ComplexHeatmap	Gu[70]	v2.22.0
htmltools	N/A	v0.5.8.1
plotly	N/A	v4.10.4
ggrepel	N/A	v0.9.6
Cairo	N/A	v1.6-2
limma	Ritchie et al.[71]	v3.62.1
DESeq2	Love et al.[72]	v1.46.0
dplyr	N/A	v1.1.4

(*Continued on next page*)

Please cite this article in press as: Grassmann et al., Stepwise epigenetic signal integration drives adaptive programming of cytotoxic lymphocytes, Immunity (2026), https://doi.org/10.1016/j.immuni.2026.01.004

Continued

REAGENT or RESOURCE	SOURCE	IDENTIFIER
TxDb.Mmusculus.UCSC.mm10.knownGene	N/A	v3.10.0
GenomicFeatures	Lawrence et al.[73]	v1.58.0
AnnotationDbi	N/A	v1.68.0
ChIPpeakAnno	Zhu et al.[74]	v3.40.0
BiocParallel	N/A	v1.40.0
RColorBrewer	N/A	v1.1-3
GenomicAlignments	Lawrence et al.[73]	v1.42.0
Rsamtools	N/A	v2.22.0
Biostrings	N/A	v2.74.0
XVector	N/A	v0.46.0
SummarizedExperiment	N/A	v1.36.0
Biobase	Huber et al.[75]	v2.66.0
MatrixGenerics	N/A	v1.18.0
matrixStats	N/A	v1.4.1
rtracklayer	Lawrence et al.[76]	v1.66.0
GenomicRanges	Lawrence et al.[73]	v1.58.0
GenomeInfoDb	N/A	v1.42.0
IRanges	Lawrence et al.[73]	v2.40.0
S4Vectors	N/A	v0.44.0
BiocGenerics	Huber et al.[75]	v0.52.0
ggplot2	Wickham et al.[77]	v3.5.1
stringr	Wickham et al.[78]	v1.5.1
FastQC	Andrews et al.[79]	v0.11.8
Trimmomatic	Bolger et al.[80]	v0.39
Bowtie 2	Langmead and Salzberg[81]	v2.4.1
Picard tools	N/A	v2.23.0
MACS2	Zhang et al.[82]	v2.2.7.1
Deeptools	Ramírez et al.[83]	v3.5.4
Samtools	Danecek et al.[84]	v1.9
HOMER	Heinz et al.[85]	v4.11
R	N/A	v4.4.2

EXPERIMENTAL MODEL AND STUDY PARTICIPANT DETAILS

Mice

All mice used in this study were housed and bred under specific-pathogen-free conditions with food and water in 12-h light–dark cycles at 72 °F with 30–70% humidity at Memorial Sloan Kettering Cancer Center and handled in accordance with the guidelines of the Institutional Animal Care and Use Committee. The following mouse strains were used in this study: C57BL/6 (CD45.2), C57BL/6 CD45.1 (CD45.1), C57BL/6 CD45.1×CD45.2, *Il12rb2*$^{-/-}$, *Klra8*$^{-/-}$ (Ly49H$^{-/-}$), CD45.1xCD45.2 (Ly49H-deficient) and *Ncr1*-GFP and *Nr4a1*-GFP. Experiments were conducted using 8–10-week-old mice or 8–16 weeks post-transplant mixed bone-marrow chimeric mice and all experiments were conducted using age- and sex-matched mice in accordance with approved institutional protocols. Both sexes were used for experiments.

MCMV virus preparation

MCMV (Smith strain) was serially passaged through BALB/c hosts three times and then salivary gland viral stocks were prepared with a homogenizer for dissociating the salivary glands of infected mice 3 weeks after infection.

Please cite this article in press as: Grassmann et al., Stepwise epigenetic signal integration drives adaptive programming of cytotoxic lymphocytes, Immunity (2026), https://doi.org/10.1016/j.immuni.2026.01.004

CellPress

METHOD DETAILS

Mixed bone-marrow chimeras

Mixed bone-marrow chimeric (mBMC) mice were generated by lethally irradiating (950 cGy) C57BL/6 CD45.1×CD45.2 animals and reconstituting with a 1:1 mixture of bone-marrow cells from WT (CD45.1) and *Il12rb2*$^{-/-}$ (CD45.2) mice. Hosts were co-injected with anti-NK1.1 (PK136) to deplete any residual donor and host NK cells. Residual CD45.1^{+}CD45.2^{+} host NK cells were excluded from all analyses. To reduce the effects of maturation, Ly49H^{-} NK cells were gated for positivity of Ly49D, an activating receptor not recognizing MCMV but instead by allogenic MHC molecules.[86]

Infections of *Nr4a1*-GFP mice and mixed bone marrow chimera

Chimerism in WT:*Il12rb2*$^{-/-}$ chimera was assessed by blood staining 1-2 weeks prior to the experiment. *Nr4a1*-GFP mice and bone marrow chimera were infected i.p. with 5 x 10^3 PFU of MCMV and analyzed at the respective time points using flow cytometry.

Isolation of mouse NK cells and flow cytometry

Spleens were dissociated with glass slides and filtered through a 100-μm cell strainer. Flow cytometry experiments were analyzed using a Cytek Aurora (Cytek Biosciences). Cell sorting was performed using a BD Aria II cytometers (BD Biosciences). Before cell sorting, NK cells were enriched by incubating whole splenocytes with the following antibodies at 10 μg/ml: CD3ε (Clone 17A2), CD4 (Clone GK1.5), CD8 (Clone 2.43), Ter119 (Clone TER-119), CD19 (Clone 1D3), Ly6G (Clone 1A8) (BioXCell). After washing, cells were incubated with goat anti-rat beads (QIAGEN, cat. no. 310107). For intracellular staining, cells were fixed and permeabilized using eBioscience Intracellular Fix & Perm Buffer Set (Thermo Fisher, cat. no. 88-8824-00). For *ex vivo* RNAseq analysis in Figure 1G, Ly49H^{-} NK cells were gated for positivity of Ly49D to reduce the effects of maturation.

Cell culture for *in vitro* experiments

NK cells and T cells were cultured in complete IMDM (10% FBS, 1× L-glutamine, 1× sodium pyruvate, 1× BME, 1× MEM-NAA and 25 mM HEPES). For cytokine stimulations, we used 50 ng/ml mouse IL-15 (Peprotech, cat. 210-15), 100U/ml IFNa (R&D, cat. 12105) and 20 ng/ml mouse IL-12 (R&D Systems, cat. 419-ML-050) depending on the experiment.

In vitro receptor and cytokine stimulation for sequencing of NK cells

High-binding 96-well flat-bottom plates were coated with 100 μl per well of 20 μg/ml anti-NK1.1 (Clone PK136, BioLegend, cat. 108759) in PBS at 4 °C overnight. To prevent antigen-receptor signaling in negative controls, we used negative enrichment via magnetic beads and Ncr1-GFP mice. Splenic NK cells from Ncr1-GFP mice were purified using the NK Cell Isolation Kit (Miltenyi, cat. 130-115-818). Depending on the condition, NK cells were stimulated for 1-3h in 96 wells coated with anti-NK1.1 or in uncoated wells. After 1-3h, NK cells were either sorted for GFP positivity and directly used for sequencing or stimulated for 3h with IL-12 (10ng/ml). RNA-seq was performed after 3h + 3h of stimulation. ATAC-seq was performed after 3h or 6h (Figure S3C). STAT1, STAT4 and STAT5 CUT&RUN was performed after 3h of aNK1.1 stimulation and 1h of IFNa, IL-12 or IL-15 stimulation. For controls, cells were incubated for 3h in uncoated wells with full media and 1h of stimulation (cytokines only). c-JUN CUT&RUN was performed after 3h of antigen stimulation. For AP1 inhibition, cells were incubated for 1h with 50uM pan-AP1 inhibitor (SR 11302, Tocris, cat. 2476) or DMSO as control, washed off and stimulated according to the respective experiment.

CTV dilution and proliferation assay

Splenocytes from CD45.1/.1 (WT1), CD45.1/.2 (WT2) and *Il12rb2*$^{-/-}$ CD45.2/.2 (*Il12rb2*$^{-/-}$) were pooled and enriched using the NK Cell Isolation Kit (Miltenyi, cat. 130-115-818). For CTV assays, cells were stained with CellTrace Violet (CTV) according to the manufacturer's instructions (Thermo Scientific, cat. C34557). NK cells were then stimulated in aNK1.1. coated plates and stimulated with cytokines according to the respective experiment, or directly pooled and injected (Figure 4H). Sequential stimulation was performed as 3h of aNK1.1 and 3h of IL-12 stimulation before adding of IL-15 for overnight incubation. For CTV assays, NK cells were kept after sequential stimulation in aNK1.1 coated 96-well U-bottom plates overnight and then re-plated in 96-well U-Bottom plates without aNK1.1 coating for an additional 2 days.

Generation of retrogenic mice

Retrogenic mice were generated as described in Straub et al.[30] Briefly, HSCs were sorted by staining with SCA-1 antibodies and expanded in DMEM containing 10%FCS, 1% Penicillin/Streptomycin, 1% L-Gln, 2ng/ml mIL-3 (Peprotech), 50ng/ml mIL-6 (Peprotech) and 50ng/ml mSCF (Peprotech) for 3 days. Retronectin coated plates were coated with retrovirus generated with HEK cells transfected with mP71 vectors and pI-ECO packaging vectors (using Lipofectamine™ LTX Reagent with PLUS™ Reagent) by centrifugation at 3000g for 2h. Cells were spinoculated for 90min at 800g, cultured for 2 additional days and injected into mice irradiated with 950 cGy prior to injection of HSCs.

Please cite this article in press as: Grassmann et al., Stepwise epigenetic signal integration drives adaptive programming of cytotoxic lymphocytes, Immunity (2026), https://doi.org/10.1016/j.immuni.2026.01.004

CD8$^+$ T cell peptide stimulation

Whole splenocytes from OT-1 mice (C57BL/6-Tg(TcraTcrb)1100Mjb/J) were seeded at a concentration of 400,000/well of a 96 well plate. Peptide (SIINFEKL = N4 or SIIQFEHL = Q4H7) was serially diluted and added. IL-12 was added at a final concentration of 10ng/ml where applicable. For CUT&RUNs and CD62L staining analysis, 10ng/ml of peptide were used.

T cell transfer and Listeria infection

Frequency of retrogenic T cells was assessed by multimer staining (SIINFEKL multimer, NIH Core Facility). T cells were sorted as CD8$^+$ CD44^{low} (naïve cells, acute expansion) or CD8$^+$ CD44^{high} (activated cells, day 8 retransfer for recall experiment) and injected into recipients i.v. Listeria-OVA was cultured in 5ml of BHI media (BD Biosciences) with Erythromycin overnight. 50ul of overnight culture was inoculated into 5ml of fresh BHI + Erythromycin and grown to an optical density (OD600) of 0.9 – 1.1. OD of 1.0 was set to correspond to a bacteria concentration of 2 x 10^8 CFU/ml. 5,000 CFU (transfer experiments) or 10,000 CFU (direct infection of retrogenics) were injected per mouse in 200ul of PBS i.v. one day after T cell injection. For acute analysis, whole spleen was pre-enriched after red blood cell lysis using negative depletion of B cells and granulocytes (anti-CD19, anti-Ly6G). Counting beads were used to calculate absolute cell number per spleen. In recall experiments, blood was collected and analyzed via flow cytometry after red blood cell lysis. Mice where one of the transferred populations had less than 3 total events were excluded.

MVAΔE5R-OVA infection

It was shown previously that deletion of E5R gene, which encodes an inhibitor of the DNA sensor, cyclic GMP-AMP synthase (cGAS), from the MVA genome, enhances antigen-specific CD8$^+$ T cell responses.[31] MVAΔE5R-OVA virus expressing mCherry were generated as described.[31] The virus was propagated in BHK-21 cells and purified through a 36% sucrose cushion. Viral titers were determined using BHK-21 cells. Mice were infected with 1 x 10^7 PFU i.p.

Single-cell RNA-sequencing and analysis

Splenic Ly49H$^+$ NK cells (CD3/TCRb/CD19−NK1.1$^+$CD49b$^+$Ly49H$^+$) from uninfected or MCMV-infected WT C57BL/6 mice were sorted as described and stained with barcoded antibodies (Total-Seq B, BioLegend). After hash-staining, NK cells were pooled and the single-cell RNA-seq from these pooled FACS-sorted cell suspensions was performed on a Chromium instrument (10x Genomics) following the user guide manual for 3′ v.3.1. In brief, FACS-sorted cells were washed once with PBS containing 1% bovine serum albumin (BSA) and resuspended in 1× PBS containing 1% BSA to a final concentration of 700–1,300 cells per μl. The viability of cells was above 80%, as confirmed with 0.2% (w/v) Trypan blue staining (Countess II). Cells were captured in droplets. Following reverse transcription and cell barcoding in droplets, emulsions were broken and cDNA-purified using Dynabeads MyOne SILANE (Thermo Fisher, cat. 37002D) followed by PCR amplification as per the manual instructions. Samples were multiplexed together on one lane of 10x Chromium (using Hash Tag Oligonucleotides (HTOs)). Final libraries were sequenced on Illumina NovaSeq6000 S4 platform (R1, 28 cycles; i7, 8 cycles; and R2, 90 cycles). The cell–gene count matrix was constructed using the 10x Cell Ranger (v7.1.0) pipeline based on mm10 2020-A reference. Viable cells were identified on the basis of library size and complexity, whereas cells with >20% of transcripts derived from mitochondria were excluded from further analysis. After mitochondrial and doublet cleanup, the raw count matrix was normalized by median library size normalization followed by log transformation. The Louvain algorithm with k = 30 was used to perform clustering and Euclidean distance was used as the metric to construct a nearest-neighbor. 'Receptor signature' was constructed from bulk RNA-seq data of naive NK cells stimulated with anti-NK1.1 for 3h *in vitro*, while 'Cytokine signature' was obtained from GSEA mouse REACTOME gene set (R-MMU-1280215). All downstream analysis was done using scanpy (v1.9.0).

RNA-sequencing

For data generated in this study, RNA was isolated from sorted cells and/or stimulated cells as described using PicoPure RNA Isolation Kit (ThermoFisher Scientific, cat. KIT0214). For *ex vivo* RNAseq analysis in Figure 1F, Ly49H$^-$ NK cells were gated for positivity of Ly49D to reduce the effects of maturation. After RiboGreen quantification and quality control by Agilent BioAnalyzer. RNA was then amplified using SMART-Seq v.4 Ultra Low Input RNA kit (Clontech, cat. 63488). Subsequently, amplified complementary DNA was used to prepare libraries with KAPA HyperPrep Kit (Kapa Biosystems, cat. KK8504). Samples were barcoded and ran on NovaSeq6000 in a 100bp/100bp paired-end run.

ATAC-sequencing

ATAC-seq was performed as described previously.[87] Briefly, sorted, stimulated cells were washed in cold PBS and lysed. The transposition reaction was incubated at 37 °C for 30 min. DNA was cleaned with the MinElute PCR Purification kit (QIAGEN, cat. 28004) and material was amplified for 5 cycles. After evaluation by real-time PCR, 8–11 additional PCR cycles were performed. The final product was cleaned by AMPure XP beads (Beckman Coulter catalog no. A63882) at a 1× ratio, and size selection was performed at a 0.5× ratio. Libraries were sequenced on a NovaSeq6000 in a 100 bp/100 bp paired-end run, using the NovaSeq6000 S2 or S4 Reagent kit (Illumina).

Please cite this article in press as: Grassmann et al., Stepwise epigenetic signal integration drives adaptive programming of cytotoxic lymphocytes, Immunity (2026), https://doi.org/10.1016/j.immuni.2026.01.004

Transcription factor CUT&RUN

For transcription factor CUT&RUN, 200,000 - 500,000 sorted total NK cells and $CD8^+$ T cells were used. T cells were sorted for homogeneous expression of activation markers (CD69 and additionally CD44 for $CD8^+$ T cells). Cells were light fixated with 0.1% PFA for 10 min, quenched with 125mM Glycine and fixated in antibody buffer (1X eBioscience Perm/Wash Buffer, 1X Roche cOmplete EDTA-free Protease Inhibitor, 0.5 uM Spermidine, + 2uM EDTA in H_2O) prior to "staining" with polyclonal anti-STAT4 (ThermoFisher, cat. 71-4500, dilution 1/100), polyclonal anti-STAT1 (Proteintech, 10144-2-AP, dilution 1/100), polyclonal anti-STAT5b (ThermoFisher, cat 71-2500, 1/100) or c-Jun (Cell Signaling cat. 9165T, dilution 1/100) antibodies. Upon antibody incubation, cells were washed twice with Buffer 1 (1X eBioscience Perm/Wash Buffer, 1X Roche cOmplete EDTA-free Protease Inhibitor, 0.5 uM Spermidine in H_2O) and resuspended in 50ul of Buffer 1 + 1X pA/G-MNase (Cell Signaling, cat. 57813) and incubated for 1h at 4°C. Cells were washed with Buffer 2 (0.05% w/v Saponin, 1X Roche cOmplete EDTA-free Protease Inhibitor, 0.5 uM Spermidine in 1X PBS) three times. After washing, Calcium Buffer (Buffer 2 + 2uM of $CaCl_2$) was used to resuspend the cells for 30 mins at 4°C to activate the pA/G-MNase reaction, and equal volume of 2X STOP Buffer (Buffer 2 + 20uM EDTA + 4uM EGTA) was added along with 1 pg of *Saccharomyces cerevisiae* spike-in DNA (Cell Signaling, cat. 29987). Samples were incubated for 15 mins at 37°C, spun down at 18,500g for 5min and supernatant was collected. DNA fragements were digested with Proteinase K (Thermo Fisher, cat. EO0491) under addition of 0.1% SDS for 4h at 65°C. DNA was isolated and purified using Qiagen MinElute Kit and subjected to library amplification using a KAPA HyperPrep Kit according to the manufacurer's protocol.[88,89] Samples were barcoded and ran on a NovaSeq6000 in a 100 bp/100 bp paired-end run.

RNA-seq, ChIP-seq, CUT&RUN, and ATAC-seq data processing

Data processing methods for published RNA-seq, ChIP-seq, and ATAC-seq datasets have been previously described.[21,57] For RNA-seq dataset generated in this study, transcript quantification was based on the mm10 University of California, Santa Cruz (UCSC) Known Gene models and performed using the quasi-mapping-based mode of Salmon (v0.13.1) correcting for potential GC bias. Transcript was summarized to gene level using tximport (v1.10.1). For ATACseq and CUT&RUN datasets found in this study, paired reads were trimmed for adaptors and removal of low-quality reads by using Trimmomatic (v0.39) and aligned to the mm10 reference genome using Bowtie2 (v2.4.1). ATACseq dataset was subjected to Tn5 correction prior to alignment. Upon alignment, peaks were called using MACS2 (v2.2.7.1) with input samples as a control using narrow peak parameters with cutoff-analysis -p 1e-5 –keep-dup all -B –SPMR. For ATAC-seq data, reproducible peaks showing an IDR value of 0.05 or less in each condition were retained, aggregated across the experiment and merged via union generate the final atlas, and annotated with the UCSC Known Gene model. Reads were mapped to the final atlas and counted with the summarizeOverlaps function from the GenomicAlignment package (v1.34.1). For CUT&RUN data, peak atlas for each antibody target was generated by merging via union of peaks called by each sample after filtering out bottom 25% of peaks by MACS2 calculated qValue. Resulting peak atlas was further filtered to only retain peaks that were called by two or more replicates within each sample group, as well as peaks that do not overlap the ENCODE's DAC Exclusion List Regions (ENCFF547MET). CUT&RUN data was normalized with two methods as indicated in figure legends. Median-of-ratios method utilized the default DESeq2 (v1.46.0) parameters to generate size factor values for normalization, with the count matrix of raw counts of the atlas peaks as input. For 3kb atlas flanking region method, 3kb of 5' and 3' flanking regions of the peak atlas were generated, only keeping the flanking regions that do not overlap with other atlas peaks. 'estimateSizeFactors' function from the DESeq2 was then used on the counts from these filtered flanking regions to generate size factor values for normalization. The rationale for using the median-of-ratios method for the STAT targets is to visualize genomic redistribution, whereas c-Jun showed a strong dependence on antigen stimulation and was therefore analyzed using the flanking method.

Motif analysis

For motif enrichment analysis, each peak in the atlas was assessed using Find Individual Motif Occurrences (FIMO) from the MEME Suite (v5.4.1) against all motifs (224) from JASPAR CORE (v2024) *Mus musculus* database. Peaks with antigen-dependent increase and decrease in STAT4 binding were compared with the total STAT4 atlas to examine motif enrichment using one-sided Kolmogorov-Smirnov (KS) test. The KS test statistic D is shown on the x-axis and the proportion of regions associated with the motif is shown on the y-axis. The odds ratio (frequency of the motif in increase or decrease group divided by its frequency in the entire atlas) was used to assign the motif to either left (regions with antigen-dependent decrease, negative value), or right (regions with antigen-dependent decrease, positive value) in x-axis. Enrichment for known motifs was assessed using HOMER (v4.11) findMotifsGenome.pl with arguments mm10 -size given -len 6,8,10,12 -mset vertebrates -mask, with background set as other peaks in the respective STAT4 peak atlas.

Downstream analyses of RNA-seq and ATAC-seq

For data generated in this study, differential analyses were executed with DESeq2 (v1.38.3) using UCSC Known Gene models as reference annotations. For RNA-seq or ATAC-seq, genes or peaks are considered differential if they showed p-adjusted value of < 0.05, adjusted for multiple hypothesis correction. Motif enrichment analysis was conducted using HOMER algorithm using regions that showed differential accessibility ($p_{adj} < 0.05$ & $|\log2 \text{ fold change}| > 0.5$) found between conditions with parameter '–size given –len 6,8,10,12,15 –mset vertebrates –mast' for de novo motif analysis. For correlation analyses, spearman coefficients were calculated using $\log_2$FC modeled by DESeq2 when comparing between conditions on either shared differential features (genes or

Please cite this article in press as: Grassmann et al., Stepwise epigenetic signal integration drives adaptive programming of cytotoxic lymphocytes, Immunity (2026), https://doi.org/10.1016/j.immuni.2026.01.004

peaks) for each condition, or all shared features. Table S1 contains a comparison of ATACseq *in vitro* (aNK1.1 vs. unstim) with *in vivo* (Nur77pos vs. Nur77neg) and peaks were classified according to significance in STAT4 CUT&RUN (aNK1.1 + IL-12 vs. IL-12).

Visualization of RNA-seq, CUT&RUN and ATAC-seq

For peak-centered heatmaps and tracks, BAM files were converted to bigwig files using bamCoverage function and scaled based on sizeFactor modeled by DESeq2 or stated methods. Scaled bigwig files from each replicate per condition were then averaged using bigwigAverage function from deepTools (v3.5.4). All heatmaps from CUT&RUN and ATAC-seq experiments were plotted using EnrichedHeatmap (v1.28.1), while heatmaps from RNA-seq data were plotted using ComplexHeatmap (v2.22.0). All genomic tracks were either visualized by GViz (v1.42.1) or IGV (v2.9.4).